UNIVERSITY OF CALIFORNIA, MERCED

Catalysis at aqueous interfaces

A dissertation submitted in partial satisfaction of the requirements

for the degree Doctor of Philosophy

In

Chemistry

by

Thuy Duy Thi Nguyen

Committee in charge:

Professor Tao Ye, Chair

Professor Ryan Baxter

Professor Son Nguyen, Advisor

Professor Yue Wang

Professor Xuan Zhang

2023

The Dissertation of Thuy Duy Thi Nguyen is approved, and it is acceptable in quality and form for publication on microfilm and electronically:

Professor Ryan Baxter	Date
Professor Yue Wang	Date
Professor Xuan Zhang	Date
Professor Son Nguyen, Advisor	Date
Professor Tao Ye, Chair	Date

University of California, Merced

2023

To my family and friends.

Table of Contents

List of Figures

List of Abbreviations

MP-SNP	mesoporous silica nanoparticles
UV-Vis	ultraviolet-visible
FTIR	Fourier-transform infrared
DEAD	diethyl azodicarboxylate
SHS	second harmonic scattering
SFG	sum frequency generation
VSFG	vibrational sum frequency generation
KIE	kinetic isotope effect
PTO	potassium titanium oxide oxalate
CTAC	cetyltrimethylammonium chloride
SDS	sodium dodecyl sulfate

Acknowledgements

I would like to thank my advisor, Dr. Son Nguyen, for his guidance and support. He played a major role in the person I have become today. I am grateful for my colleagues for helping me strengthen my knowledge and being there for me throughout my PhD journey. I thank my collaborators at UC Merced and UC Berkeley for their discussion and contribution to my project. I would like to express my special thanks to my committee members, Dr. Tao Ye, Dr. Ryan Baxter, Dr. Yue Wang, and Dr. Xuan Zhang for their feedback, advice, and support. Without them, none of this work would have been possible!

I am grateful for my friends and family for their understanding and words of encouragement that helped me get through the tough times. Their genuine support and belief in me have been my source of strength. Lastly, to my sister, you are and have been the person I look up to. I could not have done this without your unconditional support!

This work was supported by the Hellman Fellows Fund and the UC Office of the President within the Multicampus Research Programs and Initiatives (M21PL3263, M23PR5931).

Permissions

Permission to use copyrighted material that appears in Chapter 2 has been granted by the American Chemical Society. The material originally appeared in the following: Duy Nguyen, Sarah Casillas, Hnubci Vang, Anthony Garcia, Hikaru Mizuno, Erika J. Riffe, Richard J. Saykally, and Son C. Nguyen (2021) *J. Phys. Chem. Lett.* 12, 12, 3026–3030.

Permission to use copyrighted material that appears in Chapter 3 has been granted by the American Chemical Society. The material originally appeared in the following: Duy Nguyen and Son C. Nguyen (2022) *J. Phys. Chem. B*, 126, 16, 3180–3185.

Permission to use copyrighted material that appears in Chapter 4 has been granted by the American Chemical Society. The material originally appeared in the following: Duy Nguyen, Pin Lyu, and Son C. Nguyen (2023) *J. Phys. Chem. B*, 127, 11, 2323–2330.

Curriculum vitae

Thuy Duy Thi Nguyen

Education

Ph.D. Chemistry and Biochemistry 2018 – expected 2023

University of California, Merced, CA. Advisor: Dr. Son Nguyen.

B.S. Chemistry, Honor Program 2013 – 2017

University of Science, Ho Chi Minh city, Vietnam. Advisor: Dr. Phuong Tran.

Research Interests

- Catalysis at aqueous interfaces
- Nanomaterials

Research Experience

- Synthesis and functionalization of mesoporous silica nanoparticles and metallic nanoparticles.
- Studying kinetics of organic reactions at soft interfaces.

Publications

1. **Nguyen, D.,** Lyu, P., and Nguyen, S. C. (2023). Experimental and Thermodynamic Viewpoints on Claims of a Spontaneous H_2O_2 Formation at the Air-Water Interface. The Journal of Physical Chemistry B, 127 (11), 2323–2330.
2. **Nguyen, D.**, & Nguyen, S. C. (2022). Revisiting the Effect of the Air–Water Interface of Ultrasonically Atomized Water Microdroplets on H_2O_2 Formation. The Journal of Physical Chemistry B, 126(16), 3180-3185.
3. **Nguyen, D.**, Casillas, S., Vang, H., Garcia, A., Mizuno, H., Riffe, E. J., ... & Nguyen, S. C. (2021). Catalytic Mechanism of Interfacial Water in the Cycloaddition of Quadricyclane and Diethyl Azodicarboxylate. The journal of physical chemistry letters, 12(12), 3026-3030.
4. Tran, P. H., **Nguyen, T. D. T.**, Tu, T. A. T., & Le, T. N. (2020). Magnetically recoverable γ-Fe_2O_3 nanoparticles as a highly active catalyst for Friedel–Crafts

benzoylation reaction under ultrasound irradiation. Arabian Journal of Chemistry, 13(1), 290-297.

5. Nguyen, P. T., **Nguyen, T. D. T.**, Nguyen, V. S., Dang, D. T. X., Le, H. M., Wei, T. C., & Tran, P. H. (2019). Application of deep eutectic solvent from phenol and choline chloride in electrolyte to improve stability performance in dye-sensitized solar cells. Journal of Molecular Liquids, 277, 157-162.
6. Thi Nguyen, N. H., Thi Nguyen, P. P., **Thi Nguyen, T. D.**, Thi Tran, M. N., Thi Huynh, T. N., & Tran, P. H. (2017). Au Nanorod: An Efficient Catalyst for One-Pot Synthesis of 3,4-Dihydropyrimidin-2(1H)-ones via the Multicomponent Biginelli Reaction. ChemistrySelect, 2(13), 3932-3936.

Presentations

1. Duy Nguyen. Catalytic mechanism of interfacial water in the cycloaddition reaction of quadricyclane and diethyl azodicarboxylate; ACS Spring meeting. Spring 2021.
2. Duy Nguyen. Controlling "water droplets" for catalysis of on-water reactions; Chemistry and Chemical Biology Symposium; University of California, Merced, CA. May 2019.
3. Duy Nguyen, Catalytic Mechanism of Interfacial Water in the Cycloaddition of Quadricyclane and Diethyl Azodicarboxylate, University of California Chemical Symposium, Spring 2021.
4. Duy Nguyen, Kinetics Study on the Cycloaddition of Quadricyclane and Diethyl Azodicarboxylate at the Water/Organic Interfaces, UCM Research week, Spring 2020.

Teaching experience

- CHEM 008 - Principles of Organic Chemistry: Lab and discussion in Spring 2023, Fall 2021, Fall 2020, Fall 2019, and Summer 2019.
- CHEM 002 - General Chemistry II: Lab and discussion in Spring 2021 and Spring 2019.

Awards and Honors

1. Chemistry and Biochemistry Top-off fellowship, UC Merced, 2022.

2. Acknowledgements from Chemistry and Biochemistry (CBC) department, UC Merced, for the JPCB 2022 paper and the journal cover, 2022.
3. Best Graduate Student Paper Award, CBC Department, UC Merced, 2021.
4. CBC Summer Fellowship, UC Merced, 2020.

Abstract

Catalysis at aqueous interfaces

by

Thuy Duy Thi Nguyen

Doctor of Philosophy in Chemistry and Biochemistry

University of California, Merced, 2023

Many chemical reactions occurring at aqueous interfaces show different kinetics and thermodynamics than the same reactions occurring in the bulk. The nature of these chemical reactions is central in understanding environmental, industrial, and biological processes; but remains incompletely understood due to its complexity and experimental difficulties in tuning and characterizing reactions at aqueous interfaces.

In this dissertation, different experimental approaches are utilized to generate large, well-characterized aqueous interfaces for kinetic studies of chemical reactions. Chapter 1 introduces deviations of chemistry at aqueous interfaces that can alter physiochemical properties of chemical processes. In chapter 2, I study mechanistic rate accelerations of organic reactions at the organic-water interface and find that free OH groups of interfacial water molecules play an essential role in catalysis. In chapter 3, I revisit the effects of electric fields at the air-water interface of water microdroplets on directly converting water into hydrogen peroxide which is thermodynamically unfavorable in solution. Contrast to previous reports, no hydrogen peroxide production is observed in water microdroplets when tuning the electric fields at droplet surfaces. In chapter 4, I discuss claims of spontaneous hydrogen peroxide formation at the air-water interface and pinpoint potential experiments that can help to clarify them. Chapter 5 is the conclusion of the work presented in this dissertation.

Chapter 1

Introduction

Chemical reactivity at aqueous interfaces

Aqueous interfaces are ubiquitous in natural and technological processes. They connect bulk water with gaseous, liquid, or solid bodies and can create a unique environment for chemical reactions to take place.[1, 2] Many chemical reactions have showed dramatic rate accelerations at or near aqueous interfaces as compared to in bulk phase, and this phenomenon is so-called "on-water" catalysis.[2-7] Understanding the nature of these interfacial process would have great contributions to catalytic chemistry and other chemistry systems including biochemistry, atmospheric chemistry, and industry. However, the reason underlying these rate accelerations is complex and incompletely understood.[2] Interfacial effects, which originated from the change in water density, asymmetry in intermolecular interactions, and electrostatic potential, are believed to play essential roles in catalysis at aqueous interfaces. A brief review of these properties and how they can significantly alter chemical reaction kinetics and thermodynamics is mentioned below. Details about interfacial effects on chemical reactivity can be found elsewhere.[1, 2, 8-11]

Changes in water density profile at the interface create some unique features of interfacial regions that can alter chemical reactivity.[8, 12] As two phases with different densities come in to contact, the density of the interface region changes.[13-15] For example, a monotonic drop in water density, over the distance of about 1 nm, was observed at the interface when water is in equilibrium with its vapor or in contact with an immiscible liquid (see Figure 1).[8] This variation in density can result in a change in viscosity of the interfacial water medium. As we know for reactions in the bulk, viscosity can affect reaction rates as reflected in the transmission coefficient. This universal effect could have similar impacts on chemical reactions at aqueous interfaces. For example, the cis-trans photoisomerization of 3,3'-diethyloxadicarbocyanine iodide at the air-water interface showed a 2.5 time rate acceleration relative to the bulk due to a smaller friction for motion of the substrate at the air-water interface.[16]

The inhomogeneity of interfacial environment creates anisotropic intermolecular forces applied on chemical species lying there, causing deviations in molecular orientations, adsorption, and solvation at interfaces.[8] Understanding the microscopic picture of aqueous interfaces is a stepping stone to explain chemical reactivity at aqueous

interfaces. Experimental quantitative characterization of aqueous interfaces is challenging due to disorder, capillary wave, and a relatively small number of molecules occupying the interface to the molecules in the bulk.[17] However, thanks to progress in nonlinear optical spectroscopy and other molecular surface techniques, the microscopic structure of aqueous interface is being elucidated.[17] Besides, molecular dynamics simulations (MD) have also provided valuable information in this topic.[2]

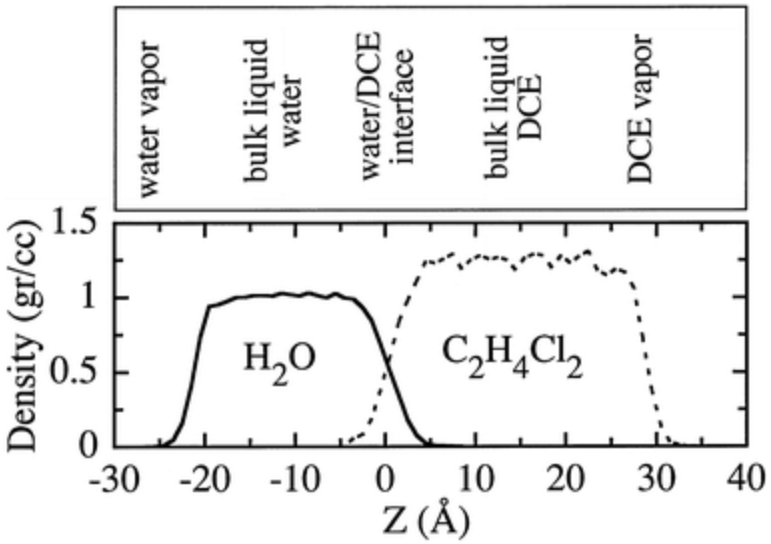

Figure 1. Density profiles of water and 1,2-dichloroethane at the liquid-liquid and liquid-vapor interface. Adapted with permission from ref. 8. Copyright © 1996, American Chemical Society.

The hydrogen bond network of water at the interface is inevitably disrupted and possesses specific orientation. Depending on the interactions between water and the second medium, water molecules reorient to lower the energy cost of breaking water hydrogen bond networks (see Figure 2). Sum frequency generation (SFG) experiments[18] and MD simulations[19, 20] reported that at the pristine air-water interface, about 20% of interfacial water molecules have dangling OH groups protruding to the vapor phase. Since these water molecules cannot form hydrogen bonds with the air, they tend to orient the hydrogen atoms or electron lone pairs toward the air to minimize the loss of hydrogen bonding interactions. At the water-CCl_4 interface, vibrational sum frequency spectroscopy (VSFS) showed that water molecules possess a net orientation with their hydrogens pointing into the CCl_4 phase.[21, 22] When it comes to water-solid interfaces, the water hydrogen bond network deviates depending on their hydrophilicity and surface charges.[23, 24] These variations in

water orientation can significantly affect interfacial structures and properties of water, hence the chemical reactions in this interfacial water solvent. Take the "on-water" reaction of quadricyclane with dimethyl azodicarboxylate as an example.[25] The dangling OH groups at the organic-water interface form approximately one more hydrogen bond with the reaction transition state than the reactants, which lowers the activation energy and so enhances the reaction rate. Roughly a five-order of magnitude increase in the rate constant was estimated for this reaction.

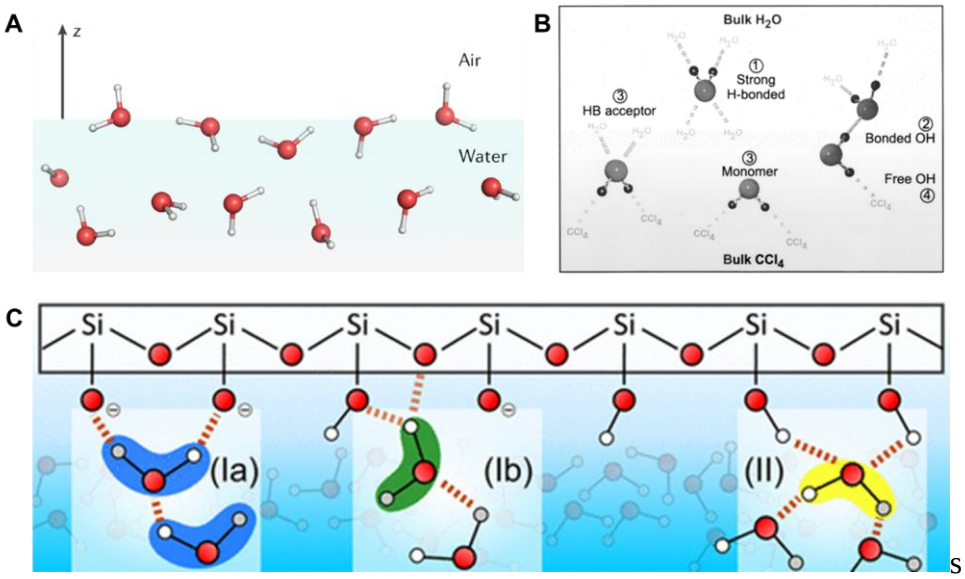

Figure 2. Water orientations at (A) air-water interface[2], (B) water- CCl_4 interface[21], and (C) silica-water interface[23]. Adapted with permission from references 2, 21, and 23. Copyright © 2020 Nature Reviews Chemistry. Copyright © 2001, American Chemical Society. Copyright © 2016, American Chemical Society.

These variations in water density and asymmetry in intermolecular forces generated from interfacial water solvent can cause changes in solvation energies of reactants, transition states, and products at aqueous interfaces. These can lead to significant effects on reaction equilibrium constants and rate constants.[8] For example, it was reported by second harmonic generation (SHG) experiments that the equilibrium constant of nitrophenol acid dissociation at the air-water interface is lowered by a factor of 50 – 100 times as compared to the bulk value.[26] This result was interpreted by a drop in solvation free energy of the ion form at the aqueous interface. Understanding adsorption and

solvation of chemical species at aqueous interfaces would give more insights into interfacial chemical reactions. Profound affinity, not only of hydrophobic organic molecules, but also polar species and even ions at aqueous interfaces have been confirmed by MD simulations and SHG experiments.[2, 27-29] However, determining absolute solvation energies of these species at the interface is a challenging task and current thermodynamic data for most chemical reactions at interfaces are unavailable. Simulations using water continuum models to quantify solvation energies of chemical species at interfacial regions often give inaccurate values. Moreover, the interfacial solvation energies also vary as the location of the solute along the normal of the interface changes. Therefore, improvement in continuum models that accounts for interfacial structure is crucial.[30, 31]

Specific orientation of water molecules at the interface creates an intrinsic electric field at the water surface, although its magnitude is still under debate.[11, 32] Recent simulations using a force field model of water reported an electric field of 10 V/nm at the air-water interface of water nanodroplets[33], which is in good agreement with experimental works on water microdroplets in oil using vibrational Stark effect[34]. This electric field can be further elevated due to preferrable adsorption of ions near aqueous interfaces.[11, 24, 33] Although the role of this interfacial electric field on chemical reactions is unclear, electric fields in general can enhance chemical reactivity and selectivity[35]. The effects of electric fields on catalysis have been long utilized in enzyme catalysis by nature[36]. It is described for a reaction with a nonpolar reactant and a dipolar transition state that the electric field would stabilize the transition state more and therefore lower the reaction barrier.[37] Utilizing electric fields for catalysis has gained more attention in chemistry although most experimental studies have mainly focused on using applied voltages to generate electric fields. The magnitude of these generated electric fields at charged electrodes[38] or scanning tunning microscope tips[39] can range from 3 to 50 V/nm. Recently, alkaline earth cations embedded in synthetic molecular systems (e.g., transition metal complexes) are also studied to generate electric field for mediating chemical reactivity.[38, 40, 41]

Studying chemical reactions at aqueous interfaces

"On-water" catalysis or rate accelerations of chemical reactions play a major part in chemistry catalysis due to the variety and abundance of aqueous interfaces.[1, 2] Since

physiochemical concepts in the bulk are not always applicable to chemistry at the interface, understanding chemistry of interfacial processes is a laborious process. Despite intensive amounts of publications, an incomplete picture of catalysis at aqueous interfaces remains.

Theoretical studies have provided indispensable information of aqueous interface properties as well as their effects on reaction kinetics and thermodynamics, yet experimental studies are always necessary. It is relatively easy to monitor bulk reactions since the total composition of the system remains constant. In contrast, interchanges of reactants and products between the interface and the adjacent bulk phase change reaction compositions at interfacial regions and monitoring them requires careful analysis. Conventional analytical methods themselves cannot classify reaction signals coming from the interface versus the bulk. Additionally, interfacial signals are often obscured by bulk signals due to a smaller number of molecules at interfaces compared to in the bulk. Therefore, using various experimental methods to characterize interfacial reactions and maximizing interfacial areas become experimentally critical. It is worth noting that sum frequency generation techniques are powerful tools to probe chemistry at interfacial regions; however, they experience difficulties in low concentration detections and experimental designs that cannot reflect native reaction conditions. Depending on reaction types and information of interests, different experimental approaches are employed.

Rate accelerations of organic reactions at water surfaces have received great attention due to its counter-intuitive nature and potential applications in green chemistry.[3, 4] A conventional way to generate organic-water interface for studying kinetics of catalysis is by vigorously mixing water and organic phase. However, this method generates an emulsion of water droplets with various sizes in oil phase. This results in fluctuations of the total interfacial area during the reaction course, hence providing unreliable reaction kinetic results. An alternative approach is supporting water phase onto silica surfaces to keep aqueous interfacial area constant for kinetic studies. More details on this topic are discussed in chapter 2.

Recent claims of formations of hydrogen peroxide at the air-water interface of water microdroplets[42] raise a question in our understanding of chemical reactions at aqueous interfaces. This is because conversion of water to hydrogen peroxide is

thermodynamically unfavorable in solution. Hydrogen peroxide is one of the most important oxidants in the air and water microdroplets are comparable in size to atmospheric water-based aerosols.[43] Therefore, more insights into this phenomenon can advance atmospheric chemistry in elucidating the presence of hydrogen peroxide and its reactions in the air. Effects of the electric field at the air-water interface of water microdroplets and thermodynamic considerations in hydrogen peroxide observations are discussed in chapters 3 and 4.

References

1. Geiger, F. M., A Virtual Issue on Aqueous Interfaces. *J Phys Chem B* **2021,** *125* (37), 10401-10403.

2. Ruiz-Lopez, M. F.; Francisco, J. S.; Martins-Costa, M. T. C.; Anglada, J. M., Molecular reactions at aqueous interfaces. *Nat Rev Chem* **2020,** *4* (9), 459-475.

3. Narayan, S.; Muldoon, J.; Finn, M. G.; Fokin, V. V.; Kolb, H. C.; Sharpless, K. B., "On water": unique reactivity of organic compounds in aqueous suspension. *Angew Chem Int Ed Engl* **2005,** *44* (21), 3275-9.

4. Chanda, A.; Fokin, V. V., Organic synthesis "on water". *Chem Rev* **2009,** *109* (2), 725-48.

5. Butler, R. N.; Coyne, A. G., Water: Nature's Reaction Enforcer-Comparative Effects for Organic Synthesis "In-Water" and "On-Water". *Chemical Reviews* **2010,** *110* (10), 6302-6337.

6. Ishiyama, T.; Tahara, T.; Morita, A., Why the Photochemical Reaction of Phenol Becomes Ultrafast at the Air-Water Interface: The Effect of Surface Hydration. *Journal of the American Chemical Society* **2022,** *144* (14), 6321-6325.

7. Kusaka, R.; Nihonyanagi, S.; Tahara, T., The photochemical reaction of phenol becomes ultrafast at the air–water interface. *Nature Chemistry* **2021,** *13*, 306-311.

8. Benjamin, I., Chemical reactions and solvation at liquid interfaces: A microscopic perspective. *Chemical Reviews* **1996,** *96* (4), 1449-1475.

9. Bjornehohn, E.; Hansen, M. H.; Hodgson, A.; Liu, L. M.; Limmer, D. T.; Michaelides, A.; Pedevilla, P.; Rossmeisl, J.; Shen, H.; Tocci, G.; Tyrode, E.; Walz, M. M.; Werner, J.; Bluhm, H., Water at Interfaces. *Chemical Reviews* **2016,** *116* (13), 7698-7726.

10. Xantheas, S. S.; Voth, G. A., Aqueous Solutions and Their Interfaces. *J Phys Chem B* **2009,** *113* (13), 3997-3999.

11. Martins-Costa, M. T. C.; Ruiz-Lopez, M. F., Electrostatics and Chemical Reactivity at the Air-Water Interface. *J Am Chem Soc* **2023,** *145* (2), 1400-1406.

12. Benjamin, I., Theory and computer simulations of solvation and chemical reactions at liquid interfaces. *Accounts Chem Res* **1995,** *28* (5), 233-239.

13. Townsend, R. M.; Gryko, J.; Rice, S. A., Structure of the Liquid Vapor Interface of Water. *Journal of Chemical Physics* **1985,** *82* (9), 4391-4392.

14. Linse, P., Monte-Carlo Simulation of Liquid Liquid Benzene Water Interface. *Journal of Chemical Physics* **1987,** *86* (7), 4177-4187.

15. Pangali, C.; Rao, M.; Berne, B., A Monte Carlo simulation of the hydrophobic interaction. *The Journal of Chemical Physics* **1979,** *71* (7), 2975-2981.

16. Sitzmann, E.; Eisenthal, K., Picosecond dynamics of a chemical reaction at the air-water interface studied by surface second harmonic generation. *The Journal of Physical Chemistry* **1988,** *92* (16), 4579-4580.

17. Jungwirth, P.; Finlayson-Pitts, B. J.; Tobias, D. J., Introduction: Structure and chemistry at aqueous interfaces. *Chemical Reviews* **2006,** *106* (4), 1137-1139.

18. Du, Q.; Superfine, R.; Freysz, E.; Shen, Y. R., Vibrational Spectroscopy of Water at the Vapor Water Interface. *Physical Review Letters* **1993,** *70* (15), 2313-2316.

19. Wilson, M. A.; Pohorille, A.; Pratt, L. R., Molecular-Dynamics of the Water Liquid-Vapor Interface. *J Electrochem Soc* **1987,** *134* (8b), C505-C505.

20. Stiopkin, I. V.; Weeraman, C.; Pieniazek, P. A.; Shalhout, F. Y.; Skinner, J. L.; Benderskii, A. V., Hydrogen bonding at the water surface revealed by isotopic dilution spectroscopy. *Nature* **2011,** *474* (7350), 192-195.

21. Scatena, L. F.; Richmond, G. L., Orientation, hydrogen bonding, and penetration of water at the organic/water interface. *J Phys Chem B* **2001,** *105* (45), 11240-11250.

22. Scatena, L. F.; Brown, M. G.; Richmond, G. L., Water at hydrophobic surfaces: Weak hydrogen bonding and strong orientation effects. *Science* **2001,** *292* (5518), 908-912.

23. Myalitsin, A.; Urashima, S.-H.; Nihonyanagi, S.; Yamaguchi, S.; Tahara, T., Water structure at the buried silica/aqueous interface studied by heterodyne-detected vibrational sum-frequency generation. *The Journal of Physical Chemistry C* **2016,** *120* (17), 9357-9363.

24. Gonella, G.; Backus, E. H. G.; Nagata, Y.; Bonthuis, D. J.; Loche, P.; Schlaich, A.; Netz, R. R.; Kuhnle, A.; McCrum, I. T.; Koper, M. T. M.; Wolf, M.; Winter, B.;

Meijer, G.; Campen, R. K.; Bonn, M., Water at charged interfaces. *Nat Rev Chem* **2021,** *5* (7), 466-485.

25. Jung, Y. S.; Marcus, R. A., On the theory of organic catalysis on water. *Journal of the American Chemical Society* **2007,** *129* (17), 5492-5502.

26. Bhattacharyya, K.; Sitzmann, E.; Eisenthal, K., Study of chemical reactions by surface second harmonic generation: p-Nitrophenol at the air–water interface. *The Journal of chemical physics* **1987,** *87* (2), 1442-1443.

27. Jungwirth, P.; Tobias, D. J., Specific ion effects at the air/water interface. *Chemical Reviews* **2006,** *106* (4), 1259-1281.

28. Petersen, P. B.; Saykally, R. J., On the nature of ions at the liquid water surface. *Annual Review of Physical Chemistry* **2006,** *57*, 333-364.

29. Vácha, R.; Slavíček, P.; Mucha, M.; Finlayson-Pitts, B. J.; Jungwirth, P., Adsorption of atmospherically relevant gases at the air/water interface: Free energy profiles of aqueous solvation of N2, O2, O3, OH, H2O, HO2, and H2O2. *The Journal of Physical Chemistry A* **2004,** *108* (52), 11573-11579.

30. Benjamin, I., Chemical Reactions and Solvation at Liquid Interfaces: A Microscopic Perspective. *Chemical Reviews* **1996,** *96* (4), 1449-1476.

31. Chang, T.-M.; Dang, L. X., Recent advances in molecular simulations of ion solvation at liquid interfaces. *Chemical Reviews* **2006,** *106* (4), 1305-1322.

32. Verreault, D.; Allen, H. C., Bridging the gap between microscopic and macroscopic views of air/aqueous salt interfaces. *Chem Phys Lett* **2013,** *586*, 1-9.

33. Hao, H.; Leven, I.; Head-Gordon, T., Can electric fields drive chemistry for an aqueous microdroplet? *Nat Commun* **2022,** *13* (1), 280.

34. Xiong, H.; Lee, J. K.; Zare, R. N.; Min, W., Strong Electric Field Observed at the Interface of Aqueous Microdroplets. *The Journal of Physical Chemistry Letters* **2020,** *11* (17), 7423-7428.

35. Shaik, S.; Danovich, D.; Joy, J.; Wang, Z. F.; Stuyver, T., Electric-Field Mediated Chemistry: Uncovering and Exploiting the Potential of (Oriented) Electric Fields to Exert Chemical Catalysis and Reaction Control. *Journal of the American Chemical Society* **2020,** *142* (29), 12551-12562.

36. Boxer, S., Electric fields and enzyme catalysis. *Abstr Pap Am Chem S* **2019,** *257*.

37. Warshel, A., Electrostatic basis of structure-function correlation in proteins. *Accounts Chem Res* **1981,** *14* (9), 284-290.

38. Gorin, C. F.; Beh, E. S.; Bui, Q. M.; Dick, G. R.; Kanan, M. W., Interfacial Electric Field Effects on a Carbene Reaction Catalyzed by Rh Porphyrins. *Journal of the American Chemical Society* **2013,** *135* (30), 11257-11265.

39. Aragones, A. C.; Haworth, N. L.; Darwish, N.; Ciampi, S.; Bloomfield, N. J.; Wallace, G. G.; Diez-Perez, I.; Coote, M. L., Electrostatic catalysis of a Diels-Alder reaction. *Nature* **2016,** *531* (7592), 88-91.

40. Leonard, N. G.; Dhaoui, R.; Chantarojsiri, T.; Yang, J. Y., Electric Fields in Catalysis: From Enzymes to Molecular Catalysts. *Acs Catalysis* **2021,** *11* (17), 10923-10932.

41. Weberg, A. B.; Murphy, R. P.; Tomson, N. C., Oriented internal electrostatic fields: an emerging design element in coordination chemistry and catalysis. *Chemical Science* **2022,** *13* (19), 5432-5446.

42. Lee, J. K.; Han, H. S.; Chaikasetsin, S.; Marron, D. P.; Waymouth, R. M.; Prinz, F. B.; Zare, R. N., Condensing water vapor to droplets generates hydrogen peroxide. *P Natl Acad Sci USA* **2020,** *117* (49), 30934-30941.

43. Zhu, C. Q.; Francisco, J. S., Production of hydrogen peroxide enabled by microdroplets. *P Natl Acad Sci USA* **2019,** *116* (39), 19222-19224.

Chapter 2

Kinetic Studies of the Cycloaddition Reaction of Quadricyclane and Diethyl Azodicarboxylate at the Organic-Water Interface

Adapted with permission from Duy Nguyen, Sarah Casillas, Hnubci Vang, Anthony Garcia, Hikaru Mizuno, Erika J. Riffe, Richard J. Saykally, and Son C. Nguyen. “Catalytic Mechanism of Interfacial Water in the Cycloaddition of Quadricyclane and Diethyl Azodicarboxylate”. *J. Phys. Chem. Lett.* **2021**, 12, 12, 3026–3030. Copyright (2021) American Chemical Society. *J. Phys. Chem. B* **2023**, 127, 11, 2323–2330

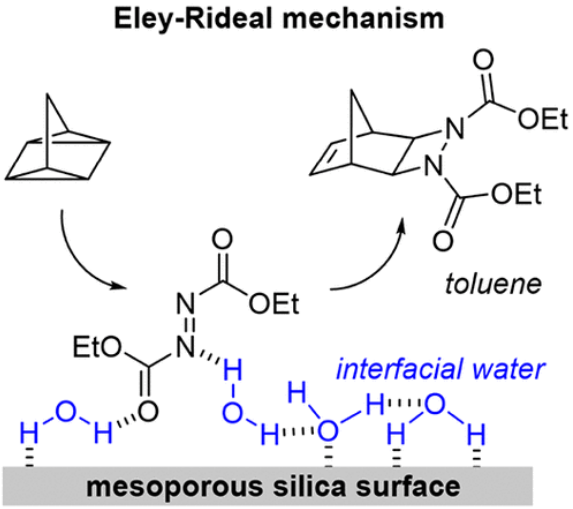

Abstract

"On-water" catalysis, the unusual activity of water molecules at the organic solvent–water interface, has been demonstrated in many organic reactions. However, the catalytic mechanism has remained unclear, largely because of the irreproducibility of the organic–water interface under the common stirring condition. Here, the interfacial area was controlled by employing adsorbed water on mesoporous silica nanoparticles as the catalyst. Reliable kinetics of the cycloaddition reaction of quadricyclane and diethyl azodicarboxylate (DEAD) at the toluene–water interface within the nanoparticle pores were measured. Data reveal an Eley–Rideal mechanism, wherein DEAD adsorbs at the toluene–water interface via hydrogen bonds formed with interfacial water, which lower the activation energy of the cycloaddition reaction. The mechanistic insights gained and preparation of surface water in silica pores described herein may facilitate the future design of improved "on-water" catalysts.

Introduction

"On-water" catalysis, catalysis of organic reactions at an organic-water interface as a heterogeneous mixture the of organic reaction solution and water was stirred, was reported by Barry Sharpless and coworkers.[1] It has been considered as a venue for inexpensive and environmentally friendly organic synthesis.[2-5] However, understanding the catalytic mechanism is still challenging,[6] largely because the stirred mixtures of organic reaction solutions and water create nonuniform water droplets that are difficult to characterize and reproduce. This issue was solved elegantly by using a biphasic fluidic platform in which the water droplets were created in polytetrafluoroethylene tubes filled with reactants and toluene, and the organic−water interfacial area was determined and correlated with reaction kinetics.[7] However, mixing within those microchannels is reduced significantly as compared to the common stirring condition in organic synthesis due to the hydrodynamically stable laminar flow.[8] Consequently, the measured reaction rate may not necessarily reflect the actual kinetic occur under the well-mixed conditions in common organic synthesis.

In this work, water was confined in mesoporous silica nanoparticles (MP-SNPs) to control the amount of interfacial water, which in turn, facilitated reliable kinetic and spectroscopic studies of the "on-water" catalyzed reaction. The cycloaddition reaction between quadricyclane and diethyl azodicarboxylate (DEAD) at the toluene−water interface serves as a prototypical reaction due to the extensive research on this reaction (Figure 5).[1, 7, 9-12] The facile tunability of the water-adsorbed MP-SNP catalyst allows for a systematic kinetic study and elucidation of the catalytic mechanism.

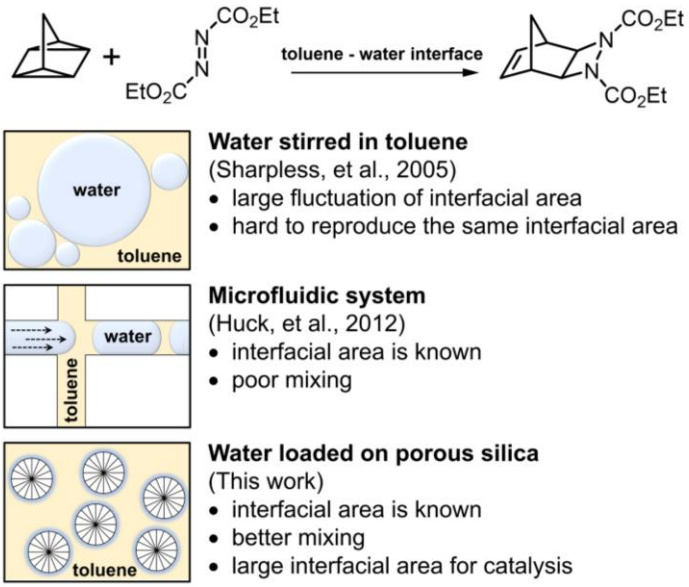

Figure 3. Development of some platforms for studies of "on-water" catalysis.

Experimental section

For a description of experimental conditions and methods used in this chapter, refer to Appendix A.

Results and Discussions

Catalytic activities of water adsorbed on mesoporous silica nanoparticles

The MP-SNPs were allowed to adsorb water vapor at room temperature in a home-built humidity-controlled box (Appendix A). FTIR spectroscopy confirmed water in the pores to be dominantly surface bound because of the characteristic red shift of the HOH bending vibration as compared to that of bulk water[13, 14] (Appendix A, Figure A2). This adsorption fashion is consistent with a previous study on mesoporous silica MCM-41 with pore sizes of 2−6 nm in which the adsorbed water spreads evenly on the surface within the pores for low amounts of adsorbed water.[15] The amount of surface water was determined by the peak area of the HOH bending mode and tuned by adjusting the adsorption time within the humidity-controlled box (Figure 6b and Appendix A). Under typical conditions

for preparing the catalyst in our kinetic studies, the adsorbed water can reach up to an average of four molecules per square nanometer of porous silica surface, which is comparable to the number of silanol groups on the same surface.[16]

To confirm that the majority of catalytic sites comprise surface-adsorbed water within the pores of MP-SNPs, the reaction conversion was monitored for three control samples in which the mass of MP-SNPs and amount of adsorbed water were kept constant, but the external surface area varied by changing the particle diameter (Figure 4c and 4d). If the reaction were to happen only on the external surface of the particles (i.e., the outermost part), the conversion would be reduced significantly for larger particles due to the reduction of external particle surface area. In fact, the observed conversions after background correction (vide infra, 27%) are strongly correlated to the internal surface areas, but not to the external surface areas (Figure 4d). This result suggests that most of the catalytic sites are within the pores. Considering the relatively small pore diameter (~2.1 nm),[17] the reactants, products, and toluene solvent can still efficiently diffuse in and out of the pores for the reaction to happen. At high water loading conditions, the conversion reaches an upper limit (Figure 4b). This suggests that water may begin to adsorb in a multilayer fashion and the percentage of active sites relative to the total amount of loaded water is reduced. Note that the reaction conversion was kept well below 100% for reliable kinetic comparisons in this study; however, a higher conversion can be achieved with longer reaction times. Nonporous SNPs prepared with adsorbed water showed lower catalytic activities due to the decreased surface area and interfacial water (Figure 4c). Dry MP-SNPs, which still have trace amounts of adsorbed water, also gave lower conversions. Because of the unavoidable trace of adsorbed water when handling the dry MP-SNPs, this trace of water, confirmed by FTIR spectroscopy (see one example in Figure A3), may partially contribute to the observed conversion. Nevertheless, the lower conversion obtained from these dry MP-SNPs indicates that the interfacial water generates greater catalytic activity than the bare silica surface. When pure water was used as the catalyst at the same loading in the reaction mixture as the water-loaded MP-SNPs (Figure A2), the conversion dropped significantly, indicating lower surface areas for water droplets. Note that the noncatalyzed reaction occurs in the bulk of toluene solvent (background reaction)

in parallel with the water catalyzed reaction occurring at the toluene−water interface. When necessary, the conversion due to noncatalyzed reaction in the bulk is subtracted from those of the catalyzed reaction. The effect of the background reaction was estimated from the noncatalyzed reaction under similar experimental conditions; this approximation is reasonable since the majority of reactant molecules exist in the bulk, as confirmed by UV−vis spectroscopy measurements on the reaction solution before and after centrifuging MP-SNPs. Given these results, MP-SNPs with an average of four water molecules per nm^2 of silica surface were selected for further kinetic study (Table A1).

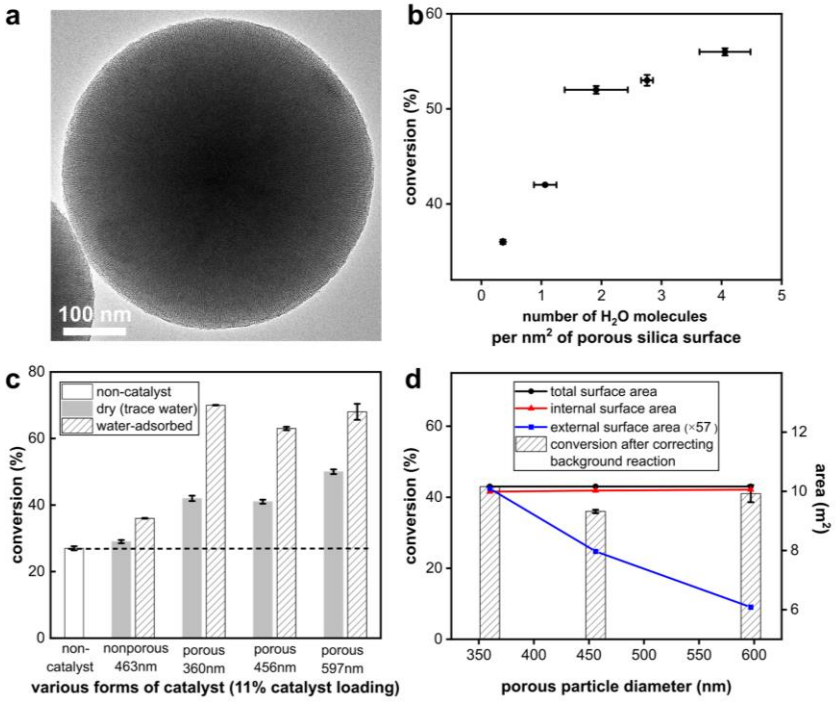

Figure 4. Water-adsorbed mesoporous silica nanoparticle catalyst for the cycloaddition of quadricyclane and DEAD. (a) Representative TEM image of 597 ± 22 nm MSNs. (b) Reaction conversion vs amount of surface water adsorbed on the silica.

Adsorption of DEAD on silica surfaces

Second harmonic scattering (SHS) spectroscopy was used to investigate the molecular interaction between DEAD and interfacial water adsorbed within the pores. In this surface specific technique, the 400 nm SHS signal generated from the 800 nm laser beam is resonantly enhanced by the strong optical absorbance of DEAD molecules (λ_{max} = 405 nm) that adsorb at the toluene−water interface within the pores. Although coherent

second harmonic generation is not allowed in bulk centrosymmetric media under the electric dipole approximation, SHS signal is still detected from our sample. The micron or submicron size centrosymmetric particles like the MP-SNPs used in this study have noncentrosymmetric local surface because the size of the particles is much larger than the coherence length of the second harmonic generation process.[18, 19] On the basis of the SHS intensity, the surface coverage of DEAD was extracted and the adsorption isotherm was shown to follow a Langmuir model (Appendix A and Figure A3). This result suggests that DEAD adsorbs at the toluene−water interface, most likely via hydrogen bonding. A control measurement on the dry porous version showed no dependence of SHS intensity on the bulk concentration of DEAD; therefore, the surface water plays a critical role in adsorption. Quadricyclane is expected not to adsorb strongly at the toluene−water interface because of its nonpolar nature.

Determining the reaction order

To determine the reaction order, initial reaction rates were measured with different initial reactant concentrations. When a reaction proceeded, a small volume of the reaction solution was extracted, diluted in cold toluene (10 °C) to quench the reaction, centrifuged to remove MP-SNPs, and the absorbance peak of DEAD at 405 nm was measured to obtain the initial reaction rate (Appendix A and Table A3). Without any catalyst, both quadricyclane and DEAD followed first-order kinetics, as expected for a homogeneous bimolecular reaction.[9] When using the catalyst, the initial rates of the catalyzed reactions were corrected by subtracting the initial rates of the corresponding background reactions. The kinetic plot in Figure 5a shows the reaction order of DEAD as pseudo-zeroth order, implying that DEAD adsorbs readily at the catalyst surface. This observation is well-aligned with the SHS results that show saturated coverage at relatively low bulk DEAD concentration. The oxygen and nitrogen atoms in DEAD are expected to form hydrogen bonds with interfacial water, and the amount of pre-adsorbed DEAD on the catalyst surface is constantly high enough to make DEAD follow pseudo-zeroth-order kinetics. Quadricyclane, however, follows closely to first-order kinetics because of its non-adsorption at the toluene−water interface. The observed dependence of reaction rate on the

catalyst surface area (i.e., proportional to the amount of surface water) also resembles first-order kinetics for the catalytic sites.

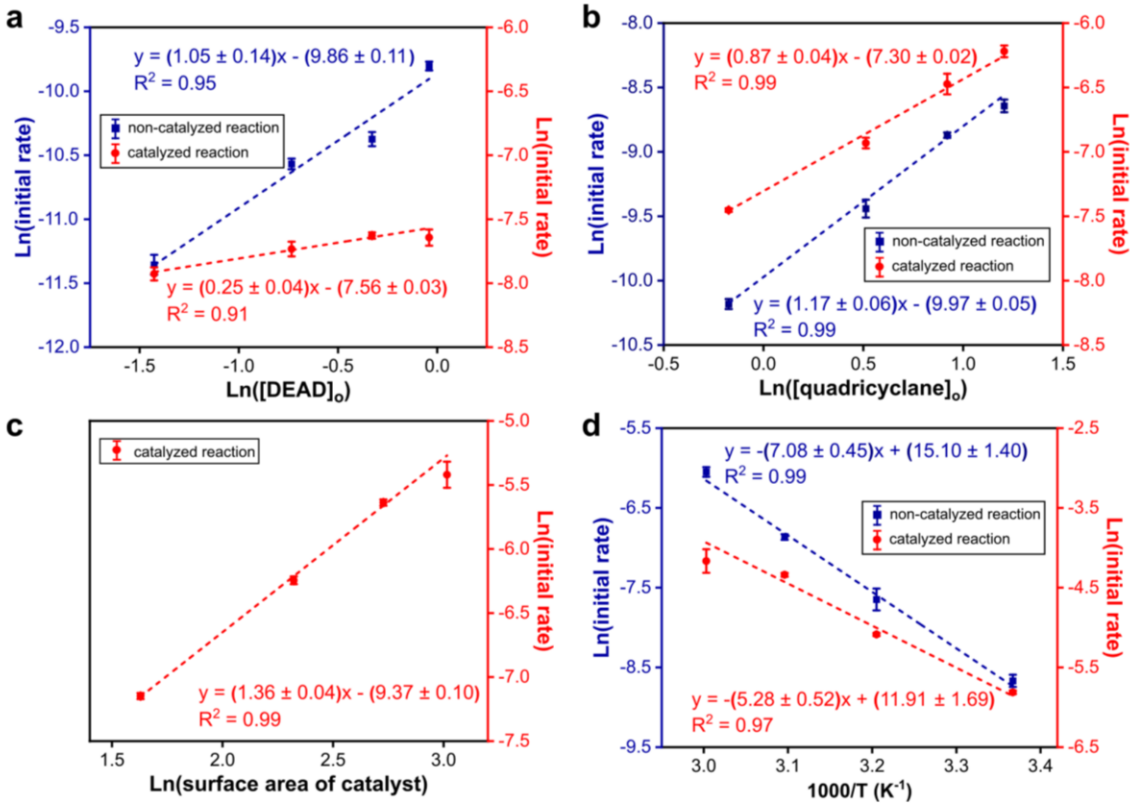

Figure 5. Kinetics of quadricyclane and DEAD reaction without catalyst (left axis) and with catalyst (right axis). (a, b, and c) Initial reaction rates with various initial concentrations of DEAD, quadricyclane, and catalyst surface area. (d) Arrhenius plots show the activation energies of noncatalyzed and catalyzed reactions to be 14.1 ± 0.9 and 10.5 ± 0.9 kcal/mol, respectively. Error bars represent one standard deviation of the means.

Determining the reaction activation energy

The apparent activation energy (E_a) of the catalyzed reaction is 10.5 ± 0.9 kcal/mol (Figure 5d), which is comparable to an estimated E_a of 12 kcal/mol for the reaction of dimethyl azodicarboxylate (DMAD) with quadricyclane in the stirring mixture of toluene and water.[1, 9] However, the E_a of the same reaction between DEAD and quadricyclane was measured as 3.9 ± 0.4 kcal/mol from the toluene−water fluidic platform,[7] likely because of the aforementioned difference between the two experimental conditions. The lowering of

the activation energy ($\Delta E_a = E_{a/withoutcatalyst} - E_{a/withcatalyst}$) with our water-loaded MPSNPs is ΔE_a = 3.6 kcal/mol, comparable to 5.4 kcal/mol determined by the toluene−water fluidic platform.[7] A previous molecular simulation reported an estimated ΔE_a of 7.5 kcal/mol for the reaction between DMAD and quadricyclane when moving the reaction from the neat solution to the aqueous interface, where the main contribution to ΔE_a is the hydrogen bonding between the surface water molecules and the transition state.[9] Considering these data, we expect that the hydrogen bonding of interfacial water contributes significantly to the observed ΔE_a. Combining the above kinetic data, the rate law for the catalyzed reaction closely follows the relationship of $(\#\text{catalytic sites})^1 \cdot [\text{quadricyclane}]^1 \cdot [\text{DEAD}]^0$.

Kinetic isotope effects

To elucidate the catalytic mechanism, possible kinetic isotope effects (KIEs) were explored by comparing the conversion when the catalyst was loaded with the same amount of water and heavy water (85% D_2O, 15% H_2O) (Appendix A, Figure A4). After 24 h of reaction, the conversions were 75% and 72% for the pure H_2O and 85% D_2O/15% H_2O loaded catalysts, respectively. Assuming the catalytic contribution of D_2O and H_2O to the total conversion is independent, the actual conversion of the presumably 100% D_2O loaded catalyst is estimated to be 71%. This small KIE of 1.1 suggests that breaking of OH bonds does not occur in the rate-determining step; this agrees with the proposed mechanism in a previous simulation that the interfacial water−DEAD hydrogen bonds lower the transition state but does not break the OH bond at the transition state.[9] This result is also consistent with an observation of k_H/k_D = 1.1 from toluene−water fluidic platform.[7] We note the original experiments by Sharpless and co-workers for the reaction between DMAD and quadricyclane showed a significant kinetic isotope effect ($k_H/k_D \sim 4.5$).[1] However, this result could arise from the uncertain surface areas of the organic solvent−water droplets. As Marcus and Jung have pointed out, many physical factors, other than the KIE, must be considered to explain this surprisingly high k_H/k_D.[9] The Diels−Alder reaction between cyclopentadiene and dimethyl fumarate has shown a KIE of 1.4, suggesting that protons transfer from water to the organic phase to catalyze the reaction.[9] However, this mechanism is not supported by our experimental data for the reaction studied here. In previous studies,

there is an assumption that the very low solubility of the organic reactants in the water phase of the organic solvent− water heterogeneous mixture may contribute to the "in-water" catalytic mechanism.[5, 20] This possibility is eliminated from our study because of the molecularly thin layer of adsorbed water on the silica surface. Finally, we would like to point out that the structure of interfacial water adsorbed in the silica pores during the course of catalysis in our experiment is currently unknown and may be somewhat different from the structure of interfacial water at the organic solvent−water interface. We hope our result will facilitate some future simulation studies to gain a clearer physical picture of this complex aqueous interface.

Proposed mechanism of cycloaddition of quadricyclane and DEAD at the water-organic interface

The proposed mechanism, here, is that the catalyzed reaction starts with the adsorption of DEAD from bulk toluene onto the interfacial water adsorbed on the silica surface, then the quadricyclane diffuses to the toluene−water interface and reacts with DEAD. The reaction occurs at the interface and hydrogen bonding discussed above lowers the activation barrier. The entire mechanism follows the Eley−Rideal process as illustrated in Figure 6. Since FTIR spectroscopy did not detect any signal from the free silanol groups in our catalyst, apparently silica only serves as a substrate for water adsorption and has no significant contribution to the catalytic mechanism.

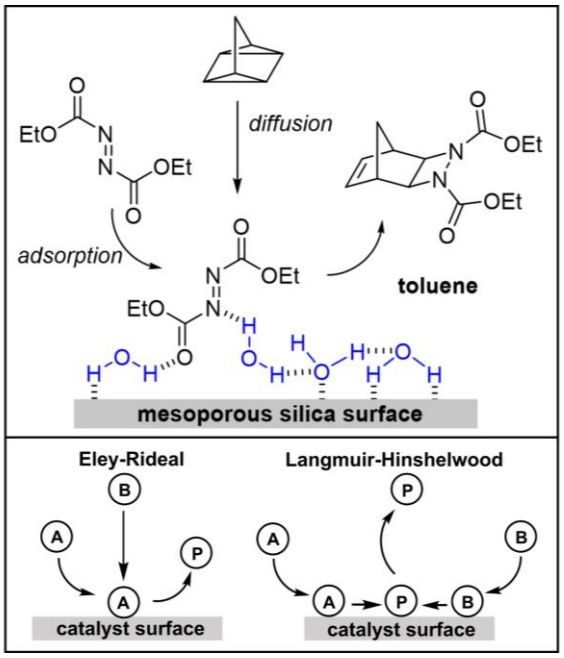

Figure 6. The Proposed Eley–Rideal mechanism for the "on-water" reaction of quadricyclane and DEAD at the toluene–water interface.

Conclusions

The highly controllable adsorption of surface water on MP-SNPs enables reliable kinetic studies of the cycloaddition reaction between quadricyclane and DEAD at the organic-water interface. The dangling OH groups at the interface were proven to play a significant role in catalysis.

Though the proposed mechanism may not apply to all organic reactions happening at the organic-water interfaces and deviate depending on reaction types, reactant structures, solvents, and so on, this work suggests a feasible way to control the water-organic interfaces for easier kinetic studies. The effects of pore size, nanoconfinement, and interfacial potential on the reaction mechanism are out of scope of this study.

References

1. Narayan, S.; Muldoon, J.; Finn, M. G.; Fokin, V. V.; Kolb, H. C.; Sharpless, K. B., "On water": unique reactivity of organic compounds in aqueous suspension. *Angew Chem Int Ed Engl* **2005,** *44* (21), 3275-9.

2. Chanda, A.; Fokin, V. V., Organic synthesis "on water". *Chem Rev* **2009,** *109* (2), 725-48.

3. Butler, R. N.; Coyne, A. G., Water: nature's reaction enforcer--comparative effects for organic synthesis "in-water" and "on-water". *Chem Rev* **2010,** *110* (10), 6302-37.

4. Romney, D. K.; Arnold, F. H.; Lipshutz, B. H.; Li, C. J., Chemistry Takes a Bath: Reactions in Aqueous Media. *Journal of Organic Chemistry* **2018,** *83* (14), 7319-7322.

5. Butler, R. N.; Coyne, A. G., Organic synthesis reactions on-water at the organic-liquid water interface. *Org Biomol Chem* **2016,** *14* (42), 9945-9960.

6. Ruiz-Lopez, M. F.; Francisco, J. S.; Martins-Costa, M. T. C.; Anglada, J. M., Molecular reactions at aqueous interfaces. *Nat Rev Chem* **2020,** *4* (9), 459-475.

7. Mellouli, S.; Bousekkine, L.; Theberge, A. B.; Huck, W. T. S., Investigation of "On Water" Conditions Using a Biphasic Fluidic Platform. *Angew Chem Int Edit* **2012,** *51* (32), 7981-7984.

8. Shang, L. R.; Cheng, Y.; Zhao, Y. J., Emerging Droplet Microfluidics. *Chemical Reviews* **2017,** *117* (12), 7964-8040.

9. Jung, Y. S.; Marcus, R. A., On the theory of organic catalysis on water. *Journal of the American Chemical Society* **2007,** *129* (17), 5492-5502.

10. Beattie, J. K.; McErlean, C. S. P.; Phippen, C. B. W., The Mechanism of On-Water Catalysis. *Chem-Eur J* **2010,** *16* (30), 8972-8974.

11. Bain, R. M.; Sathyamoorthi, S.; Zare, R. N., "On-Droplet" Chemistry: The Cycloaddition of Diethyl Azodicarboxylate and Quadricyclane. *Angew Chem Int Edit* **2017,** *56* (47), 15083-15087.

12. Guo, D. M.; Zhu, D. Y.; Zhou, X. H.; Zheng, B., Accelerating the "On Water" Reaction: By Organic-Water Interface or By Hydrodynamic Effects? *Langmuir* **2015,** *31* (51), 13759-13763.

13. Gallas, J. P.; Goupil, J. M.; Vimont, A.; Lavalley, J. C.; Gil, B.; Gilson, J. P.; Miserque, O., Quantification of Water and Silanol Species on Various Silicas by Coupling IR Spectroscopy and in-Situ Thermogravimetry. *Langmuir* **2009,** *25* (10), 5825-5834.

14. Benesi, H. A.; Jones, A. C., An Infrared Study of the Water-Silica Gel System. *J Phys Chem-Us* **1959,** *63* (2), 179-182.

15. Grunberg, B.; Emmler, T.; Gedat, E.; Shenderovich, I.; Findenegg, G. H.; Limbach, H. H.; Buntkowsky, G., Hydrogen bonding of water confined in mesoporous silica MCM-41 and SBA-15 studied by 1H solid-state NMR. *Chemistry* **2004,** *10* (22), 5689-96.

16. Shenderovich, I. G.; Buntkowsky, G.; Schreiber, A.; Gedat, E.; Sharif, S.; Albrecht, J.; Golubev, N. S.; Findenegg, G. H.; Limbach, H. H., Pyridine-N-15 - A mobile NMR sensor for surface acidity and surface defects of mesoporous silica. *J Phys Chem B* **2003,** *107* (43), 11924-11939.

17. Yano, K.; Fukushima, Y., Synthesis of mono-dispersed mesoporous silica spheres with highly ordered hexagonal regularity using conventional alkyltrimethylammonium halide as a surfactant. *J Mater Chem* **2004,** *14* (10), 1579-1584.

18. Cole, W. T. S.; Wei, H. Y.; Nguyen, S. C.; Harris, C. B.; Miller, D. J.; Saykally, R. J., Dynamics of Micropollutant Adsorption to Polystyrene Surfaces Probed by Angle-Resolved Second Harmonic Scattering. *J Phys Chem C* **2019,** *123* (23), 14362-14369.

19. Wang, H. F.; Yan, E. C. Y.; Liu, Y.; Eisenthal, K. B., Energetics and population of molecules at microscopic liquid and solid surfaces. *J Phys Chem B* **1998,** *102* (23), 4446-4450.

20. Zuo, Y. J.; Qu, J., How Does Aqueous Solubility of Organic Reactant Affect a Water-Promoted Reaction? *Journal of Organic Chemistry* **2014,** *79* (15), 6832-6839.

Chapter 3

Revisiting the Formation of H_2O_2 at the Air-Water Interface of Water Microdroplets

Adapted with permission from Duy Nguyen and Son C. Nguyen. “Revisiting the Effect of the Air–Water Interface of Ultrasonically Atomized Water Microdroplets on H_2O_2 Formation”. *J. Phys. Chem. B* **2022**, 126, 16, 3180–3185.

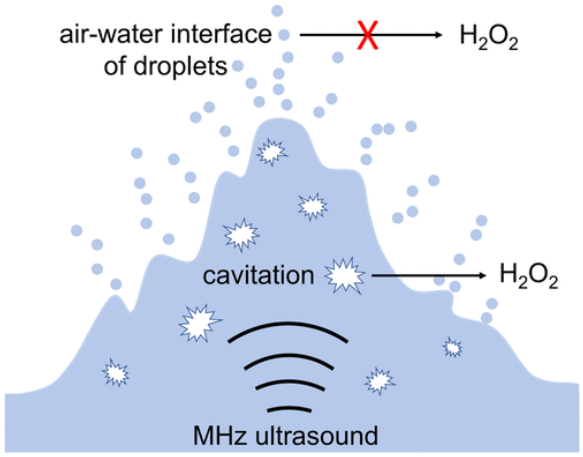

Abstract

Studying chemical processes at the air–water interface is always challenging. A recent report claimed that H_2O_2 was formed spontaneously on the surface of condensed water microdroplets. However, a newer report concluded that the detected H_2O_2 in the previous report could originate in part from the water vapor source that involved ultrasonic atomization of liquid water. Here, this phenomenon is reinvestigated regarding the influence of ultrasonic cavitation, surface modification of droplets, and solutes in the bulk liquid on H_2O_2 production. When the droplet surfaces were modified by surfactants, H_2O_2 production did not change, whereas adding gases or inorganic compounds to the bulk solution caused significant changes in H_2O_2 production. These results confirm that H_2O_2 formation originates from cavitation in bulk solutions. It is concluded that the air–water interface of water microdroplets itself does not generate H_2O_2.

Introduction

Air−water interfaces are expected to favor some chemical processes, as compared to the bulk solution,[1-3] yet gathering more experimental evidence is still challenging. Recently, Zare and co-workers reported that H_2O_2 was formed spontaneously when condensing water vapor from the air onto inert substrates to form water droplets, and a strong electric field existing at the air−water interface of the droplets was suggested as the origin of H_2O_2 formation.[4] Shortly afterward, Mishra and co-workers pointed out that H_2O_2 production in the previous experiment was an experimental artifact.[5] They contrasted H_2O_2 detection for water droplets produced from condensing two separate sources of water vapor: one generated by an ultrasonic humidifier as similarly used in Zare et al.'s study[4] and another created by gently heating water. The droplets condensed from the former did contain H_2O_2, while the latter did not. While there are discrepancies in the detected amount of H_2O_2 between these two early studies, the observed phenomenon deserves more confirmation from different approaches and considerations. In this paper, the production of H_2O_2 by the ultrasonic mist maker (also known as a humidifier) was studied and discussed relative to the two previous works (Figure 7). More importantly, H_2O_2 formation was reinvestigated as to whether it originates from the air−water interface of the water droplets. Unlike the previous experiments, wherein the ultrasonic humidifier created water droplets, which in turn were allowed to evaporate at room temperate to provide water vapor for later condensation, our experiments directly utilized these droplets to avoid any potential side effects from the substrates or environmental contaminations (Figure 7 and Figure 8a). The water droplet surfaces were then modified by adding surfactants to the bulk solution, and the effect of surface modification on H_2O_2 formation was examined.

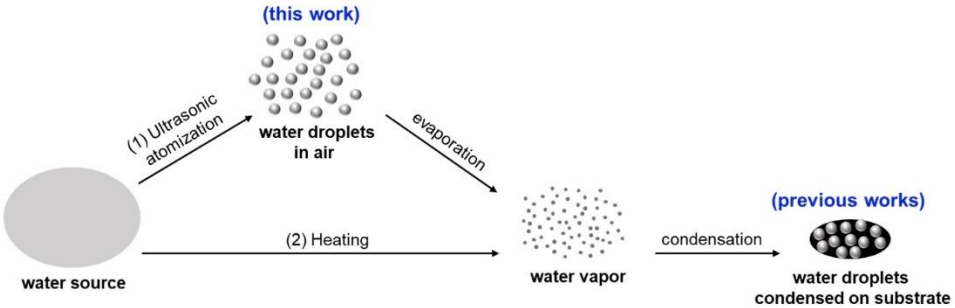

Figure 7. Platforms for studies of H_2O_2 formation from water droplets

Experimental section

For a description of experimental conditions and methods used in this chapter, refer to Appendix B.

Results and Discussions

Effect of Ultrasound on H_2O_2 Formation

First, the effect of ultrasound on H_2O_2 formation in our setup was investigated. In both samples shown in 6a, propagation of ultrasonic waves from the transducers through the water baths and the polypropylene tubes created acoustic cavities in the tubes. H_2O_2 was detected in both samples A and B (Figure 8b). The explanation for this result is sonolysis of water and thermolysis of dissolved O_2 to create active radicals such as $^{\bullet}H$, $^{\bullet}OH$, and $^{\bullet}OOH$, which in turn react to form H_2O_2 and H_2.[6-8] These processes are driven by very high temperatures and pressures of the localized hot spots, which are formed when these cavities collapse. Although sonochemistry is usually carried out at frequencies of 10–100 kHz,[7] and the fact that a 1.7 MHz frequency used in this and the two previous studies[4, 5] should create less energetic cavities than those commonly used frequencies,[7, 9] the 1.7 MHz source is still sufficient to drive sonochemistry in water and create H_2O_2. We herein provide a precautionary alert that ultrasonic humidifiers used as household products can generate traces of H_2O_2. Sample A with an open water surface and sample B with an isolated surface were utilized to compare the effect of protuberances and droplets on H_2O_2 formation. As shown for sample A, the acoustic radiation force creates a protuberance at the water surface and the coherent interaction between the waves incident on and reflected from the water surface results in the formation of numerous cavitation bubbles within the protuberance (see illustration in Figure 8c).[10] According to cavitation-wave theory,[10] acoustic emissions from the cavitation bubbles along with capillary waves on the water surface enhance the breaking of capillary wave crests and facilitate the pinch-off of droplets. For sample B, the water surface is isolated by the stopper, which prevents

the formation of protuberances and droplets. The amount of H_2O_2 generated in samples A and B is quite different and the difference results from the fact that sample A has both protuberance and droplets. Since the formations of the protuberance and water droplets are inseparable, it is impossible to evaluate the relative significance of the cavities in the protuberance and the air–water interface of the water droplets in H_2O_2 formation. If the air–water interface of the water droplets produced H_2O_2, the droplets would finish their lifecycle (in the order of seconds before falling back to the bulk solution) in the tube and therefore would also increase the amount of H_2O_2 in the bulk solution.

As mentioned above, Mishra and co-workers confirmed that cavitation generated by the ultrasonic humidifier contributes to H_2O_2 production and that the air–water interface of the condensed water droplets does not produce H_2O_2.[5] Thus, at this point, the explanation for our results in sample A, as well as their results, is that the protuberance creates a high concentration of cavities, which crucially contribute to the observed H_2O_2 production. Sample B has cavitation, but there is no protuberance for concentrating cavities, resulting in low H_2O_2 production. Besides, sample A has a better gas mixing due to the open surface and protuberance's dynamic, hence more O_2 is dissolved for more H_2O_2 formation. Note that Mishra and co-workers' conclusions were drawn from analyzing droplets condensed from the water source that evolved ultrasonic irradiation; therefore, the current work focusing on the ultrasonically atomized droplets should follow the same principle. To reconfirm and gain more insights into this phenomenon, we chemically modified the surface of water droplets to evaluate its effects on H_2O_2 production.

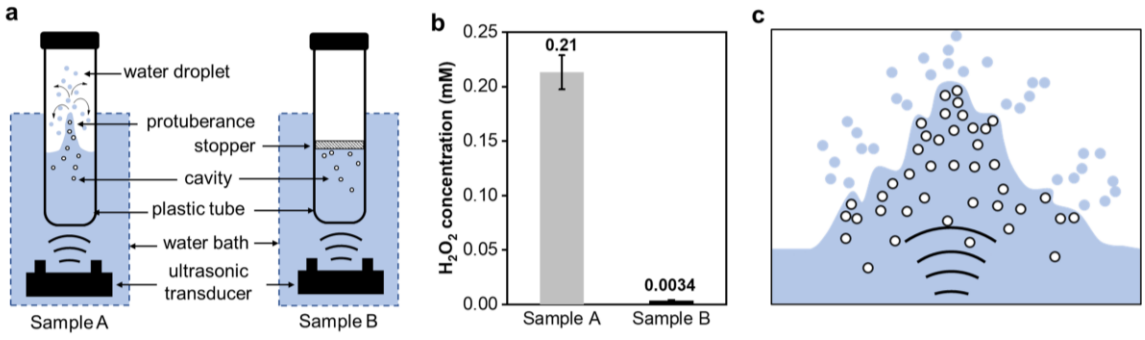

Figure 8. Formation of H_2O_2 from ultrasonic irradiation of water. (a) Experimental setup with both open and isolated surface water. (b) Detected H_2O_2 in 3 mL of water in samples A and B after 6 h irradiation by 1.7

MHz ultrasound. The 3 mL water in sample A or B absorbs an ultrasound power of 1.28W (c) Depiction of acoustic cavitation and ultrasonic atomization when focused ultrasound encounters the water surface in sample A. Sample B has cavitation, but not protuberances nor droplets.

Effect of the air-water interfaces on H_2O_2 formation

To be independent of Mishra and coworkers' conclusions,[5] we initially hypothesize that both cavitation and droplet surfaces contribute to H_2O_2 formation. As we confirmed above, the former clearly creates H_2O_2, and the latter is discussed below. In a set of experiments similar to that on sample A, surfactant solutions with concentrations well below the critical micelle concentrations were added into the tubes; we expected that the surfactants would alter the pristine air−water interface of the droplets but not the cavitation dynamics in the solution.[11, 12] Cationic, anionic, and nonionic surfactants, such as cetyltrimethylammonium chloride (CTAC), sodium dodecyl sulfate (SDS), and triton X-100, respectively, were used to modify the surface of water droplets. As ionic surfactants adsorbed at water droplet surfaces, they create electric double layers and eventually strong electrostatic fields at these surfaces. Nonionic surfactants are not our focus as they adsorb at the surfaces but do not create electrostatic fields. A control experiment with triton X-100 solution was conducted to validate whether its adsorption to the water droplet surface could alter H_2O_2 formation. This control experiment yielded a similar amount of H_2O_2 to the pure water sample (see Appendix C, Figure A21). We then focus on experiments with ionic surfactants. It was reported that at the concentration of above 50 μM for both dodecyl trimethylammonium bromide (similar structure to CTAC) and SDS, these surfactants effectively adsorb at surfaces of cavitation bubbles and partially quench •OH radical production, thereby reducing H_2O_2 production.[7, 11] As the concentration of surfactants was set in the range of 5 nM−50 μM in our experiment, we can ensure that H_2O_2 formation from cavitation is the same for all samples presented in Figure 9. This condition allows us to evaluate only the influence of the air−water interface on H_2O_2 production.

For a surfactant solution with a bulk concentration of 50 μM, the surface coverage is less than 10% of the maximum surface coverage.[13] Since the ultrasonically atomized droplets are pinched off from the bulk, they have a comparable surfactant concentration to

the bulk concentration. As the droplets in our experiment are quite large, about 7.2 ± 3.3 μm in diameter (Figure A14, Appendix C), their surface coverage is expected to be close to the surface coverage of a flat surface of a bulk surfactant solution. Also, previous studies showed that despite this low surface coverage, surfactants are still capable of altering the pristine air−water interface.[13, 14] In those studies, vibrational sum frequency generation spectroscopy on the air−water interfaces of similar surfactant solutions with a comparable concentration and surface coverage showed that interfacial water molecules experience a large electrostatic field, resulting in a strong alignment, as compared to those at a clean air−water interface.[13, 14] The presence of ionic surfactants and their counterions at the interfaces creates ionic double layers that induce a much stronger electric field than the neat air−water interface does.[13, 15] Therefore, it is expected that the interfacial water in the surfactant-added water droplets should experience a larger electric field. According to Zare and co-workers,[4] the electric field at the air−water interface is the driving force for ionizing OH^- anions and forming •OH radicals. Eventually, the radicals recombine to form H_2O_2. In our work, as we increased the surfactant concentration, we expected a rise in the strength of the electric field at the interface; however, we did not see any noticeable changes in H_2O_2 production (Figure 9). Note that our control experiments confirmed that the presence of surfactants does not interfere with H_2O_2 characterization by the PTO method. The oxygen of the interfacial water molecules points toward the air for the cationic surfactant or toward the bulk for the anionic version (see Figure 9a).[16] Note that this description is already simplified as the local water molecules near the interface may form hydrogen bonds with the SDS head groups and not have well alignments with the electric field. When moving from one surfactant to another, the electric field flips and interfacial water molecules change their orientation; however, we did not see any influence on H_2O_2 production. These results indicated that modifications of the air−water interface of water droplets have no effect on H_2O_2 production, which leads to the conclusion that H_2O_2 formation does not depend on the electric field at the air−water interface.

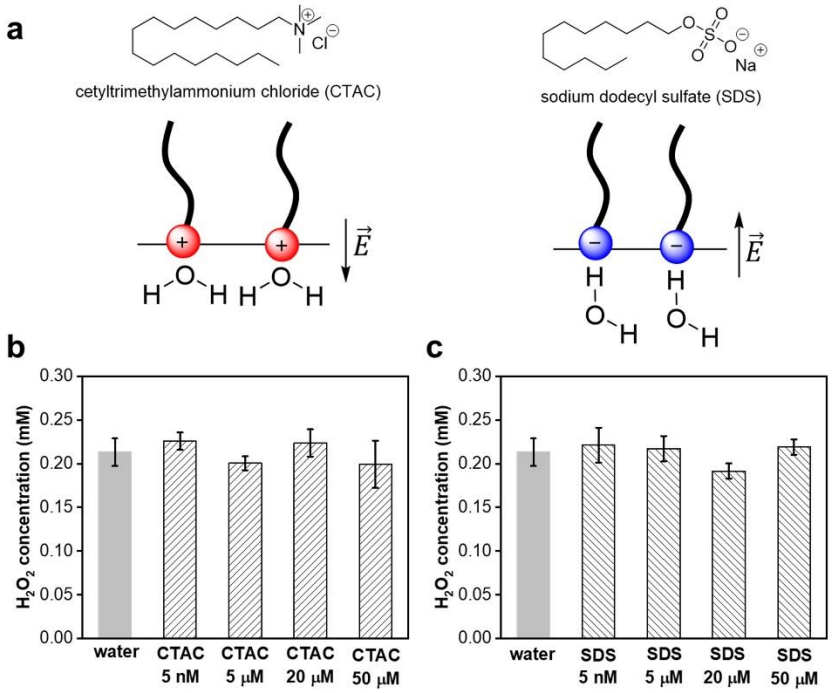

Figure 9. Modifying droplet surfaces with surfactants does not change H_2O_2 production. (a) CTAC and SDS surfactants used in this study and the simplified presentations of their enhancement of the electrostatic field and water orientation near the interface as compared to the clean air–water interface. Note that the hydrogen bonds between the water molecules and surfactant head groups may interfere with the well alignment of water with the electric field. (b, c) H_2O_2 production when using CTAC and SDS at different bulk concentrations. Reaction conditions: 3 mL of surfactant solution, 6 h irradiation of 1.7 MHz ultrasound at room temperature. Error bars represent one standard deviation of the mean.

Effect of Solutes in the Bulk Liquid on Formation of H_2O_2

In contrast, the bulk concentration of dissolved oxygen and inorganic compounds in water liquid has large effects on H_2O_2 production. With regard to inorganic solutions used in this study, it is known that KCl and NaOH solutions have a depletion of their ions at the air−water interface, while HCl and NaSCN solutions have the opposite effect for H^+, Cl^-, and SCN^-.[17, 18] These ion adsorption and desorption at air−water interfaces are insignificant when their bulk concentrations are well below 1 M. Their adsorption at the water surface is much weaker than the adsorption of surfactants. Thus, we expect that these inorganic compounds do not cause surface modification of the water droplets, and their behavior in the bulk is more important as they interfere with the sonochemistry of water.

These solutes can react with ˙H and ˙OH radicals initially generated from water sonolysis and influence the combination path of ˙OH, therefore forming more or less H_2O_2 (Figure 10a).[7] Figure 10b shows that H_2O_2 formation increases with the amount of dissolved oxygen in bulk water (see Appendix C and Table A4 for concentrations of dissolved oxygen). The O_2 is expected to diffuse into the cavitation bubbles where it can undergo thermolysis to form oxygen atoms, which can then react with water to form the ˙OH radical. The O_2 could also react with hydrogen atoms to form the hydroperoxyl radical, which can combine with the ˙OH radical to form H_2O_2 (see Figure 10a).[6, 19] The nonvolatile solutes react with hydrogen atoms and ˙OH radicals at the boundary of the cavities or in the bulk after the cavities collapse.[20] As demonstrated in eqs 3 and 4 in Figure 10a and experimental data for KCl and HCl solutions in Figure 10c, the Cl^- ion in low-pH solution quenches ˙OH radicals, leaving fewer ˙OH radicals for producing H_2O_2. As expected, the SCN^- ion also quenches ˙OH radicals, resulting in lower production of H_2O_2 (see eq 5 in Figure 10a). In contrast, the OH^- ions in NaOH solution quench hydrogen atoms, which favors H_2O_2 formation (see eq 6 in Figure 10a). More experimental data and explanations are provided in Figure A18 and Table A5 in Appendix C. All these results confirm that cavitation in the bulk is the origin of H_2O_2 formation.

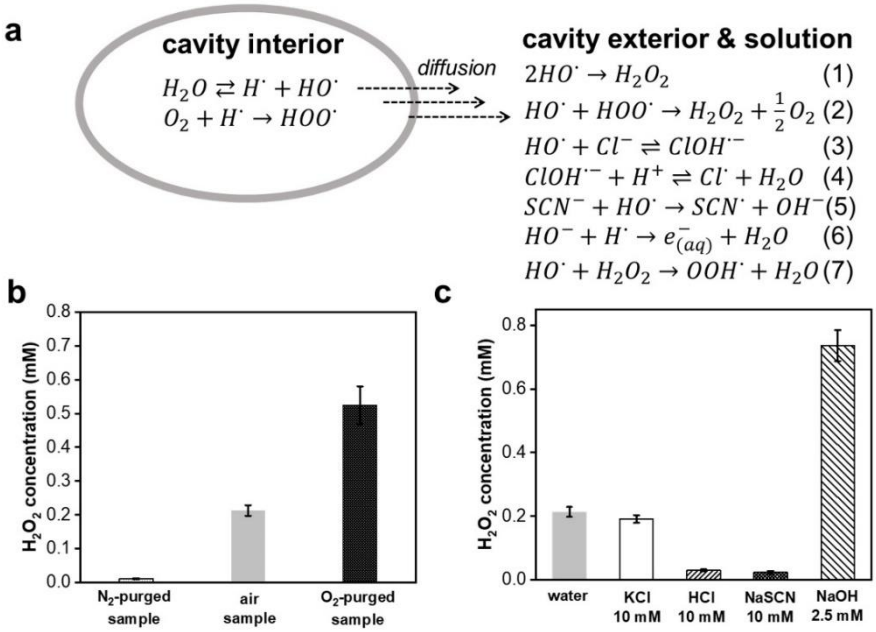

Figure 10. H_2O_2 production when using different solutes in the bulk liquid. (a) Chemical processes during cavitation. (b, c) H_2O_2 production when using various gases and inorganic compounds. Reaction conditions: 3 mL of aqueous solution, 6 h irradiation of 1.7 MHz ultrasound at room temperature. Error bars represent one standard deviation of the mean.

Relating to the Results Observed in Previous Works

Combining all the above experimental evidence, we conclude that the air−water interface does not produce H_2O_2 and that the detected H_2O_2 comes from sonolysis of water. The ultrasonic humidifier used in Zare et al.'s study[4] must generate H_2O_2, and this H_2O_2 evaporated from either the water reservoir (the part that experiences the ultrasound) of the humidifier or the atomized droplets. Eventually, the vapor H_2O_2 might co-condense with the water vapor to form water droplets on the substrates, resulting in detection of H_2O_2 in the condensed droplets. Unfortunately, the exact kinetics of H_2O_2 formation from the humidifier in that study is unknown to us, hence we cannot use our understanding to completely interpret the experimental results in that work.

We do, however, attempt to provide some insights that could generally explain the previous observation. Zare and co-workers observed a rise and fall in H_2O_2 production when the microdroplets grew. The rise could come from the increasing amount of H_2O_2 vapor being fed to the gas chamber in their experiment when the humidifier was turned on. Our kinetic study shows that the rate of producing H_2O_2 is high at the early operating time of the humidifier (see Figure A19), and then, the production reaches a plateau because H_2O_2 can quench the •OH radical efficiently[21] and suppress any further formation of H_2O_2 (see eq 7 in Figures 8c and A20). The fall of H_2O_2 detection at later times of condensation (i.e., 2−10 min as reported) in that study could come from a slower rate of H_2O_2 condensation on the water droplets as the condensation progressed. Note that H_2O_2 has a boiling point of 150 °C, and thus, it condenses faster than water at the early times of the condensation. We suspect that higher H_2O_2 detection observed for higher humidity in Zare et al.'s study[4] could come from the condition that the ultrasonic humidifier was allowed to run for a longer time, and it fed more H_2O_2 to the chamber storing water vapor. The

variation in condensation conditions affects H_2O_2 concentrations observed in condensed water droplets.

There is a discrepancy in H_2O_2 detection between Mishra (reported as ~1 μM)[5] and Zare (0.5−3.9 ppm or 15−115 μM)[4] groups, probably because the former used a much larger chamber (a glovebox) that diluted H_2O_2 concentration in the air, resulting in less H_2O_2 condensing in water droplets. In our experiment, the amount of detected H_2O_2 is much larger (~220 μM after 6 h irradiation) because the ultrasonic irradiation is longer, and our simple experimental design avoids losses of H_2O_2 during condensation. In a related study,[22] Zare and co-workers also reported that H_2O_2 was detected from water droplets produced via pneumatic spraying. However, Mishra and co-workers stated that air-borne ozone, pre-existing in the environment, is the source of H_2O_2 formation.[5] The sprayed water droplets have high surface areas for higher mass transfer of ozone into water, and the decomposition of ozone in water can form H_2O_2. In control experiments without air-borne ozone, Mishra and coworkers did not detect H_2O_2 in sprays (detection limit > 250 nM), and they concluded that the air−water interface did not spontaneously produce H_2O_2. Although we used interface modification to study the phenomenon as a different approach, our conclusion is well-aligned with their conclusion.

Conclusions

H_2O_2 detection described in the previous report[4] is expected to depend on the conditions of ultrasonic irradiation and the properties of the bulk solution used in the ultrasonic humidifier. We proved the correlation between cavitation energy and H_2O_2 generation. Modifying the surface with ionic surfactants is expected to change surface potential, hence electric field of water droplets. However, no effects on H_2O_2 were observed. The droplet air−water interface generating H_2O_2 in the previous study may result from an experimental artifact.

References

1. Zhong, J.; Kumar, M.; Anglada, J. M.; Martins-Costa, M. T. C.; Ruiz-Lopez, M. F.; Zeng, X. C.; Francisco, J. S., Atmospheric Spectroscopy and Photochemistry at Environmental Water Interfaces. *Annual Review of Physical Chemistry, Vol 70* **2019,** *70*, 45-69.

2. Wei, Z. W.; Li, Y. J.; Cooks, R. G.; Yan, X., Accelerated Reaction Kinetics in Microdroplets: Overview and Recent Developments. *Annual Review of Physical Chemistry, Vol 71* **2020,** *71*, 31-51.

3. Ruiz-Lopez, M. F.; Francisco, J. S.; Martins-Costa, M. T. C.; Anglada, J. M., Molecular reactions at aqueous interfaces. *Nat Rev Chem* **2020,** *4* (9), 459-475.

4. Lee, J. K.; Han, H. S.; Chaikasetsin, S.; Marron, D. P.; Waymouth, R. M.; Prinz, F. B.; Zare, R. N., Condensing water vapor to droplets generates hydrogen peroxide. *P Natl Acad Sci USA* **2020,** *117* (49), 30934-30941.

5. Musskopf, N. H.; Gallo, A.; Zhang, P.; Petry, J.; Mishra, H., The Air-Water Interface of Water Microdroplets Formed by Ultrasonication or Condensation Does Not Produce H2O2. *J Phys Chem Lett* **2021,** *12* (46), 11422-11429.

6. Beckett, M. A.; Hua, I., Impact of ultrasonic frequency on aqueous sonoluminescence and sonochemistry. *J Phys Chem A* **2001,** *105* (15), 3796-3802.

7. Thompson, L. H.; Doraiswamy, L. K., Sonochemistry: Science and engineering. *Ind Eng Chem Res* **1999,** *38* (4), 1215-1249.

8. Riesz, P.; Berdahl, D.; Christman, C. L., Free-Radical Generation by Ultrasound in Aqueous and Nonaqueous Solutions. *Environ Health Persp* **1985,** *64*, 233-252.

9. Petrier, C.; Lamy, M. F.; Francony, A.; Benahcene, A.; David, B.; Renaudin, V.; Gondrexon, N., Sonochemical Degradation of Phenol in Dilute Aqueous-Solutions - Comparison of the Reaction-Rates at 20-Khz and 487-Khz. *J Phys Chem-Us* **1994,** *98* (41), 10514-10520.

10. Simon, J. C.; Sapozhnikov, O. A.; Khokhlova, V. A.; Crum, L. A.; Bailey, M. R., Ultrasonic atomization of liquids in drop-chain acoustic fountains. *J Fluid Mech* **2015,** *766*.

11. Alegria, A. E.; Lion, Y.; Kondo, T.; Riesz, P., Sonolysis of Aqueous Surfactant Solutions - Probing the Interfacial Region of Cavitation Bubbles by Spin Trapping. *J Phys Chem-Us* **1989,** *93* (12), 4908-4913.

12. Ashokkumar, M.; Guan, J. F.; Tronson, R.; Matula, T. J.; Nuske, J. W.; Grieser, F., Effect of surfactants, polymers, and alcohol on single bubble dynamics and sonoluminescence. *Phys Rev E* **2002,** *65* (4).

13. Gragson, D. E.; McCarty, B. M.; Richmond, G. L., Ordering of interfacial water molecules at the charged air/water interface observed by vibrational sum frequency generation. *Journal of the American Chemical Society* **1997,** *119* (26), 6144-6152.

14. Nguyen, K. T.; Nguyen, A. V.; Evans, G. M., Interfacial Water Structure at Surfactant Concentrations below and above the Critical Micelle Concentration as Revealed by Sum Frequency Generation Vibrational Spectroscopy. *J Phys Chem C* **2015,** *119* (27), 15477-15481.

15. Hua, W.; Verreault, D.; Allen, H. C., Surface Electric Fields of Aqueous Solutions of NH4NO3, Mg(NO3)(2), NaNO3, and LiNO3: Implications for Atmospheric Aerosol Chemistry. *J Phys Chem C* **2014,** *118* (43), 24941-24949.

16. Baryiames, C. P.; Garrett, P.; Baiz, C. R., Bursting the bubble: A molecular understanding of surfactant-water interfaces. *Journal of Chemical Physics* **2021,** *154* (17).

17. Jungwirth, P.; Tobias, D. J., Specific ion effects at the air/water interface. *Chemical Reviews* **2006,** *106* (4), 1259-1281.

18. McCaffrey, D. L.; Nguyen, S. C.; Cox, S. J.; Weller, H.; Alivisatos, A. P.; Geissler, P. L.; Saykally, R. J., Mechanism of ion adsorption to aqueous interfaces: Graphene/water vs. air/water. *P Natl Acad Sci USA* **2017,** *114* (51), 13369-13373.

19. Hua, I.; Hoffmann, M. R., Optimization of ultrasonic irradiation as an advanced oxidation technology. *Environmental Science & Technology* **1997,** *31* (8), 2237-2243.

20. Petrier, C.; Jeunet, A.; Luche, J. L.; Reverdy, G., Unexpected Frequency-Effects on the Rate of Oxidative Processes Induced by Ultrasound. *Journal of the American Chemical Society* **1992,** *114* (8), 3148-3150.

21. Buxton, G. V.; Greenstock, C. L.; Helman, W. P.; Ross, A. B., Critical-Review of Rate Constants for Reactions of Hydrated Electrons, Hydrogen-Atoms and Hydroxyl Radicals (.Oh/.O-) in Aqueous-Solution. *J Phys Chem Ref Data* **1988,** *17* (2), 513-886.

22. Lee, J. K.; Walker, K. L.; Han, H. S.; Kang, J.; Prinz, F. B.; Waymouth, R. M.; Nam, H. G.; Zare, R. N., Spontaneous generation of hydrogen peroxide from aqueous microdroplets. *P Natl Acad Sci USA* **2019,** *116* (39), 19294-19298.

Chapter 4

Experimental and Thermodynamic Viewpoints on Spontaneous H_2O_2 Formation at the Air-Water Interface of Water Microdroplets

Adapted with permission from Duy Nguyen, Pin Lyu, and Son C. Nguyen. "Experimental and Thermodynamic Viewpoints on Spontaneous H_2O_2 Formation at the Air-Water Interface". *J. Phys. Chem. B* **2023**, 127, 11, 2323–2330.

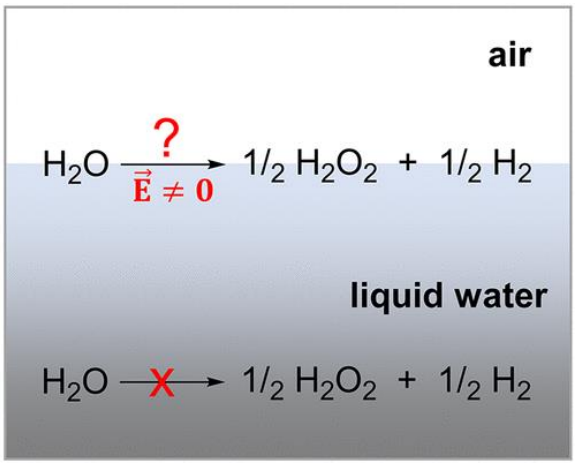

Abstract

Recent claims of the spontaneous H_2O_2 formation at the air–water interface of water microdroplets have sparked debates on its feasibility. New results from different research groups have provided more insight into these claims, but conclusive proofs are still far from realized. In this Perspective, thermodynamic viewpoints, potential experiments, and theoretical approaches are presented as references for future studies. We suggest that future work should seek for H_2 byproduct as indirect evidence to confirm the feasibility of this phenomenon. Examining potential energy surfaces for H_2O_2 formation reaction when moving from the bulk to the interface under the influence of the local electric fields is also critical to establish this phenomenon.

Introduction

Thermodynamics and kinetics of many chemical reactions at interfaces are different from those in the bulk.[1-5] These differences come from the inhomogeneity of the media at or near the interfaces. As for the air-water interface, surrounding water imposes asymmetric molecular interactions on the observed water molecules and on solutes. The interfacial water has a lower density than bulk water, and its density fluctuations give rise to macroscopic capillary waves, surface roughness and tension. These cause deviations in molecular dynamics, orientations, hydrogen bond networks, and dielectric properties from bulk water.[5, 6] In the case ions or surfactants adsorbed at the air-water interface, these modify surface tension, surface potential, and eventually interfacial chemistry.[7-9] Recently, it was reported that the surface of water microdroplets spontaneously produced H_2O_2, and the local electric field at the surface was claimed to be the driving force.[10, 11] These reports generated considerable attention because H_2O_2 formation from pure water is thermodynamically unfavorable in bulk water, and the effect of electric fields on H_2O_2 formation is still unsettled. It is essential to investigate these claims because the air-water interface is ubiquitous in nature and technologies. Understanding the chemistry at the air-water interface would advance our knowledge in aerosol and environmental chemistry. In this perspective, we discuss the inconsistent experimental results from pioneering groups and lay out some potential approaches to evaluate and understand the putative H_2O_2 presence in the studied water microdroplets.

Early reports on H_2O_2 formation from water microdroplets

Chemical reactions at air-water interfaces have been widely studied in the context of interfacial water playing the role of a reaction solvent.[1-3, 6] However, two recent reports, here called Reports 1 and 2, claimed the H_2O_2 formation at the air-water interface of water microdroplets without any additives.[10, 11] This is a big surprise because thermodynamic data suggests that H_2O_2 formation from pure liquid water is highly unfavorable. Note that research on air-water interfaces of microdroplets still generates many disagreements.[12-14] Taking the debate on acid-base character of surface water as an example, electrophoresis of air bubbles in water and electrospray ionization mass spectrometry of aqueous droplets

suggested the excess of hydroxyl ions at the air-water interfaces.[14, 15] In contrast, sum frequency and second harmonic generation spectroscopies on flat surfaces of aqueous solutions suggested the presence or enhancement of hydronium ions at the surfaces.[16-19] These spectroscopic results were well supported by many simulations.[20-22] One main factor leading to these disagreements comes from different methods used to probe the chemistries at the interfaces. Claims in Reports 1 and 2 are not exempt from debate due to reproducibility, contamination, and the lack of reasonable mechanistic interpretations.[23-25]

In Report 1, 30 μM H_2O_2 was detected from water microdroplets produced via pneumatic spraying, using silica capillary tubes and N_2 nebulizing gas (see summary in Figure 11).[10] Control experiments with O_2 nebulizing gas or dissolved O_2 in the water source did not enhance the H_2O_2 formation. Smaller droplets, created by increasing nebulization gas pressure, gave more H_2O_2. In Report 2, the water microdroplets were created by condensing water vapor on various inert substrates, and the vapor was supplied by an ultrasonic humidifier. This method of creating water droplets could avoid some undesired effects of spraying liquid, such as electrokinetics[26] or charge separation during aerodynamic breakup[27], which potentially generate H_2O_2. As we will point out later, using an ultrasonic humidifier may create cavitation and sonolysis in the water reservoir that generates H_2O_2 which later contaminates the water vapor and the studied droplets. Similar to Report 1, the amount of H_2O_2 in the collected droplets was quantified by titration with potassium titanium oxalate. Depending on experimental conditions, H_2O_2 detection could achieve in a range of 15 to 115 μM. Apparently, the reported H_2O_2 presence in water droplets was easily observed by non-sophisticated equipment, yet it is still challenging to define the underlying reason. Considering that the air-water interface is so ubiquitous, these reported results may imply that the chemical processes creating H_2O_2 might have involved interfacial chemistry we have been studying. As these two reports have gained great attention, the experiments described therein were revisited with rigorous control.

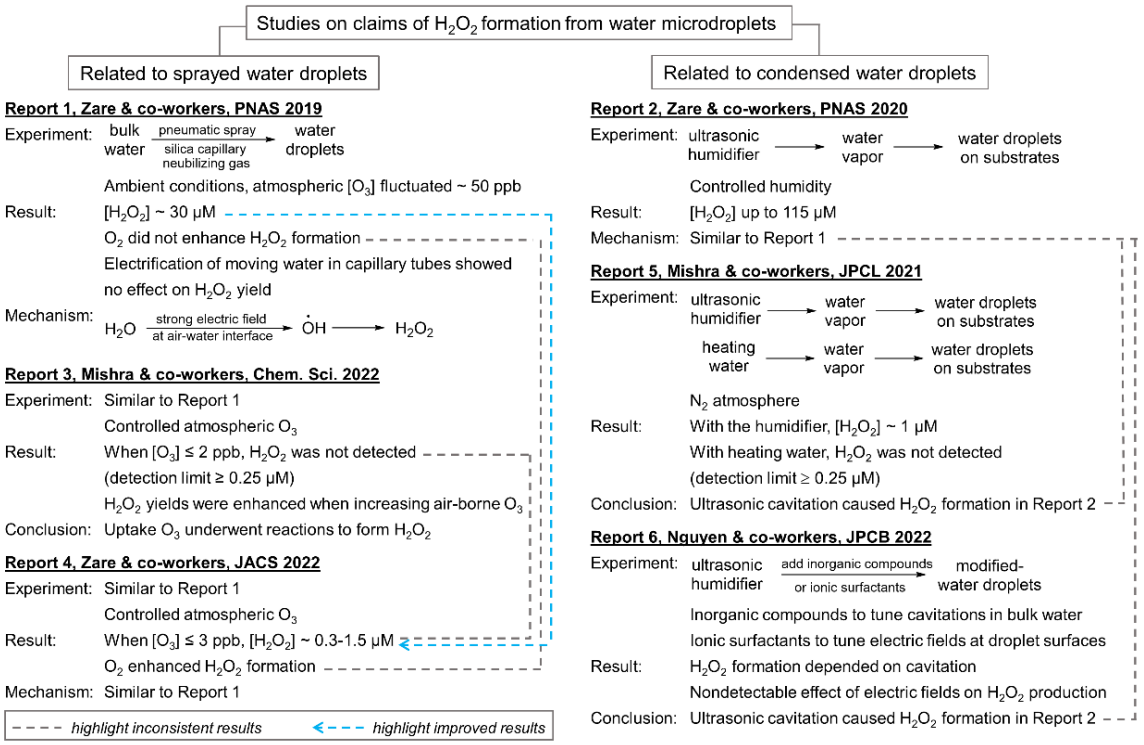

Figure 11. Recent studies on the claims of H_2O_2 formation from water droplet surfaces. Report 1[10], 2[11], 3[28], 4[29], 5[30], and 6[31] are listed as some representative works.

Revisited works with rigorous control and new insight

With regard to experiments utilizing sprayed droplets, it was soon realized that H_2O_2 yield is very sensitive to airborne O_3.[23-25, 28] The O_3 could adsorb on the droplets and undergo further reactions to form H_2O_2. As summarized in Scheme 1, experiments in Report 1 were revisited in Report 3 and 4. When O_3 was scrubbed off from the gas phase to a few ppb level, Report 3 concluded that the spray droplets had no detectable of H_2O_2 by spectrofluorometric assay[28] (detection limit ≥ 0.25 μM), but Report 4 confirmed an amount of 0.3-1.5 μM by NMR and spectrofluorometric spectroscopies[29]. Note that experiments in Report 1 did not have atmospheric O_3 removed, and the gas phase of those air-exposed experiments could have O_3 fluctuated around 50 ppb based on the daily data from Environmental Protection Agency.[32]

Since Reports 3 and 4 utilized the same method to generate water droplets under rigorous controls, their inconsistent results raise concerns about reproducibility and

deserve more attention. In Report 3, a careful analysis of mechanical vibrations and shock waves during pneumatic spraying assured that the rises of local temperature and pressure were too mild to trigger a chemical transformation. Other control experiments showed that the evaporative concentration during pneumatic spray could increase the amount of contaminated H_2O_2 in the water source up to about 10 times in the droplets, depending on the flow rates of liquid water and the nebulizing gas. This implies that trace of contaminated H_2O_2 in the water source could stay below the detection limit and pass a rigorous examination of the input, but it could later undergo evaporative concentration to reach a detectable level in the droplets. Although Report 4 used silica capillary tubes and did not confirm the effect of the capillary wall on H_2O_2 formation, a recent work from the same group reported that the water-silica contact actually produced H_2O_2.[33] In this microfluidic setup, water was flowed through channels containing a silica glass substrate, and the H_2O_2-sensitive water-soluble probe (10-acetyl-3,7dihydroxyphenoxazine) showed a H_2O_2 concentration of 56 μM. Thus, further investigation is needed to ascertain the contributions of water-solid contact, associated with evaporative concentration, to the observed H_2O_2 in spray experiments.

With regard to experiments utilizing condensed droplets, Reports 5 and 6 raised a concern that the water vapor source in Report 2 already had H_2O_2 due to ultrasonic cavitation in the used humidifiers, and this H_2O_2 co-condensed with water vapor or adsorbed on the droplets.[30, 31] According to Report 5, when the water vapor was prepared by gently heating water liquid as a control, there was no detection of H_2O_2 (detection limit ≥ 0.25 μM).[30] But when the vapor was prepared by a ultrasonic humidifier, the collected droplets had about 1 μM of H_2O_2. Based on this contrast, Report 5 concluded that the humidifier, not the droplet interfaces, contributed to H_2O_2 formation. The 1 μM is smaller than the 115 μM measured in Report 2, which could be due to a larger chamber used in Report 5 that diluted H_2O_2 concentration in the gas phase and resulted in less H_2O_2 condensing in water droplets.[31] Report 6 used a different approach by modifying the surface of ultrasonically atomized droplets with various surfactants, but those modifications did not affect H_2O_2 production. The results indicate that the droplet surface does not produce H_2O_2. Other control experiments utilizing aqueous solutions with

different gases and electrolytes confirmed that the H_2O_2 yield was only affected by sonochemistry in the bulk water.[31]

As we have learned from these exciting reports, the chemistry at air-water interface is very interesting, but quite challenging to study due to its sensitivity to contamination. Revisited experiments with better control conditions were very helpful to clarify these observations. Besides, reporting all experimental details was critical for reproducibility and further investigation. Although previous experiments were conducted under rigorous conditions to avoid any interference or contamination as much as possible, Report 4 confirmed H_2O_2 formation at the air-water interface from water droplets while Reports 3, 5 and 6 did not. Therefore, further experiments, probably with different approaches, are needed to evaluate the claims of spontaneous H_2O_2 formation at water droplet surfaces.

One desirable experiment is detecting H_2 gas as the byproduct of H_2O_2 formation from water droplets.[23] Indeed, H_2 gas is the most obvious product after balancing the self-reaction of water for generating H_2O_2, thus detection of H_2 gas can indirectly prove the H_2O_2 formation. Furthermore, the detection of H_2 gas can also rule out the potential contamination to the H_2O_2 formation, such as aforementioned O_3. In addition to those suggested experiments, the thermodynamic aspects of the H_2O_2 formation also need more investigations. Moving forward, more systematic approaches are needed to tackle these claims.

Moving forward: some potential new approaches

Detection of H_2O_2 and H_2

To evaluate the claims mentioned above, further proofs of H_2O_2 and H_2 produced are still needed. Besides eliminating contamination, quantifying these species at low concentrations is also a challenging task. One way to overcome this is to accumulate enough products for detection. As we have learned from the aforementioned work, the water droplets were first formed and H_2O_2 was later detected from the collected droplets. These procedures actually utilized kinetic methods, wherein the product concentration was monitored after a certain reaction time. Kinetic methods have certain advantages. If the amount of H_2O_2 produced at the air-water interfaces is low, it can accumulate and be

detected in the droplet after a sufficient time. Especially, the accumulation of H_2 gas is more crucial for detection due to its dispersion in the gas phase. Note that H_2 may not be produced with the presence of O_3 or O_2 contaminants (see equations 3 and 4 in Appendix 4). Furthermore, varying experimental conditions and correlating with H_2O_2 product yield can help with interpreting the reaction mechanism, such as changing droplet size to evaluate the effect of the droplet curvature, or changing experiment temperatures to estimate the reaction activation energy.

Another approach is preparing droplets with probing chemicals such that their reactions indicate the existence of H_2O_2[10, 34] or intermediates in H_2O_2 formation, e.g. hydroxyl radicals[35]. This method not only indirectly proves H_2O_2 formation but also demonstrates the influence of H_2O_2 and hydroxyl radicals on other reactions.

The kinetic method, however, has its drawbacks, such as not directly detecting reaction intermediates nor probing properties of air-water interfaces. Some interface-sensitive spectroscopies, such as sum-frequency generation (SFG)[36], can potentially probe intermediates or H_2O_2 product at water droplet surfaces. Recent glancing-angle Raman spectroscopy on 1 M H_2O_2 solution confirmed the surface propensity of H_2O_2 at the water-air interface with the standard free energy adsorption of -1.2 kcal/mol.[37] This adsorption energy had also been predicted by MD simulations.[38, 39] However, the low concentrations of these species could be a challenge for detection.

Thermodynamic considerations of H_2O_2 formation from water droplets

The claims on spontaneous formation of H_2O_2 from water droplets invite thermodynamic considerations. A table of thermodynamic quantities of chemical species that could be relevant to this reaction is provided in Appendix 4 for any future investigations. As H_2 is the expected byproduct, we use the $H_2O_{(l)} \rightarrow ½\ H_2O_{2(aq)} + ½\ H_{2(g)}$ reaction to establish our thermodynamic viewpoints. Starting from thermodynamic data, this reaction in the bulk has a standard Gibbs free energy ($\Delta G^o_{bulk\ rxn}$) of 40.7 kcal/mol (see the calculation in the SI), and it does not spontaneously occur. The same reaction in the gas phase has a ΔG^o of 42.1 kcal/mol. Note that the reactions between water and O_2 or O_3 to form H_2O_2 in liquid water have the ΔG^o_{rxn} of 24.6 or -14.4 kcal/mol, respectively (see eq.

3 and 4 in the Appendix 4). These values are significantly less positive, or even become negative, as compared to the 40.7 kcal/mol of the water self-reaction mentioned above. Thus, O_2 and O_3 contaminants must be eliminated from future studies.

Figure 12a illustrates an educated-guess pathway to demonstrate the endothermic reaction of water into H_2O_2 and H_2 in solution. In order for this reaction to happen spontaneously at the air-water interface, the reaction potential energy surface (PES) must shift in favor of the products (i.e., $\Delta G^{o}_{rxn\ at\ interface} < 0$). In other words, when moving from bulk to interfaces, the energy levels of the reactant and products must be changed as contrasted in the left and right panels in Figure 12b. Although the reaction pathway is still not known in detail and is not the focus of our thermodynamic standpoint, the emphasis in Figure 12 is the relative Gibbs free energy of the reactant and products. Hence, there are only three possibilities that could explain the spontaneous formation of H_2O_2 from water droplets. Either the Gibbs free energy of H_2O increases or those of H_2O_2 and H_2 decreases, or both when moving from bulk to the interface. Note that MD simulations showed that water molecules have almost the same free energy profile as they are in liquid or at the air-water interface.[38] H_2O_2 is energetically -1.2 kcal/mol more favorable at the air-water interface (as compared to its free energy in liquid water) as measured recently by glancing-angle Raman spectroscopy.[37] MD simulations showed that H_2O_2 and other small molecule gases such as N_2 and O_2 are about -1 kcal/mol more favorable at the air-water interface than in water.[38] H_2 is expected to have a comparable energy profile. Combing these thermodynamic data, the reaction of $H_2O_{(l)} \rightarrow ½\ H_2O_{2(aq)} + ½\ H_{2(g)}$ at the air-water interface is expected to have a lower free energy of the products by roughly about -1 kcal/mol as compared same reaction in the bulk. This energy shift is unlikely to overcome the 40.7 kcal/mol mentioned above. Future work, especially simulations, can help to re-evaluate these estimations and elucidate the feasibility of this phenomenon.

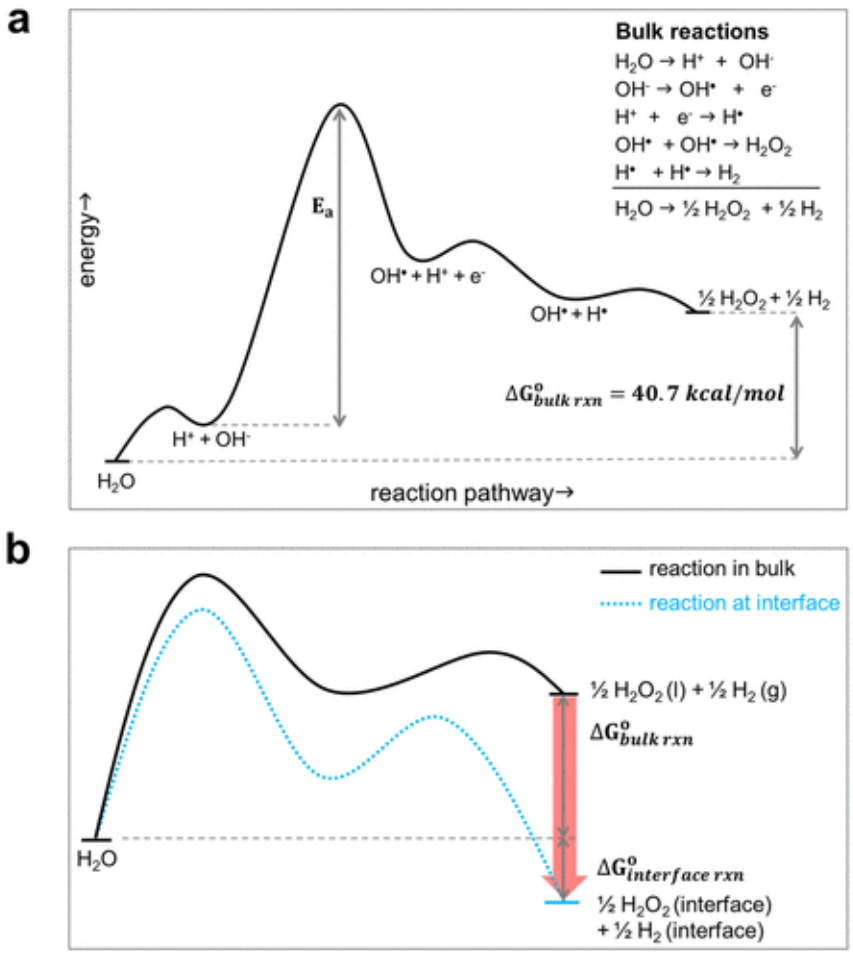

Figure 12. (a) A possible pathway to demonstrate the uphill H_2O_2 formation reaction from bulk water. (b) To make this reaction happen spontaneously at the air–water interface, the reaction pathway must be shifted to favor the products when moving from water bulk to surface. Current thermodynamic data do not support this energy shift. The red arrow indicates possible shifts in energy levels when moving from bulk to the interface.

Considerations of the proposed mechanism of H_2O_2 formation from water droplets

Understanding the mechanism of H_2O_2 formation from water microdroplets is probably the most challenging task. It is difficult to find a straightforward molecular interpretation for dramatically shifting the reaction pathway illustrated in Figure 12b. Reports 1 and 2 propose that the local electric field at the air-water interface is strong enough to ionize hydroxide ions ($^-$OH) into hydroxyl radicals (·OH), and the radicals then can combine to form H_2O_2. Report 1 also suggests that the reduction potential of H_2O_2,H^+/H_2O couple could be lower at the interface than in the bulk due to the

interface/bulk difference in solvation energy.[10, 40] This proposed ·OH pathway provides a very good starting point for further mechanistic studies because $^{-}$OH and ·OH are probably the best guesses for the starting material and intermediate, respectively. The vertical ionization energies (VIEs) of $^{-}$OH are much smaller than those values of H_2O for both gas and liquid phases.[41] Note that the VIEs of $^{-}$OH and H_2O at the water microdroplet surface are still unknown but we can expect that they follow the same trend as in gas and bulk phases. MD simulations for 4-nm water droplets show that the VIE distribution of surface $^{-}$OH are bimodal. One major peak is close to the experimental VIEs in the bulk and the extra peak is about a hundred of kcal/mol lower.[41] Hence, the water-ionization pathway for H_2O_2 formation is unlikely to happen.

The effect of the electric field on the PES of a reaction has recently gained attention, mostly in the context of reducing the activation energy, but not so much about changing the ΔG of a reaction. For enzyme catalysis, it is proposed that the active sites can be electrostatically pre-organized to stabilize the transition states of the catalyzed reactions and effectively reduce the reaction activation energy.[42] For example, the wild-type ketosteroid isomerase can exert an electric field of 144 MV/cm on the C=O bond involved in the transition state.[42] Designing local electric fields to shift the PES and improve catalytic activity or selectivity will be a new toolbox in chemical synthesis.[43-45] However, to validate claims of H_2O_2 formation in Reports 1 and 2, the two key questions needed to be addressed are: i) how strong is the local electric field at the water droplet surface? ii) can this electric field, potentially in combination with other surface effects (mentioned in the Introduction), shift the reaction PES to favor H_2O_2 product at the interface?

How strong is the electric field at the air-water interfaces of water droplets?

At a certain time and location at the interfaces, an interfacial water molecule must experience a local electric field induced by the neighbor molecules. However, it is still quite challenging to probe this electric field at the air-water interfaces of the droplets by experiments. Recently, an electric field of around 10 MV/cm at the oil-water interface of aqueous microdroplets was observed using a nitrile-bearing fluorescent probe and stimulated Raman excited fluorescence microscopy.[46] However, adding spectators to probe the electric field strength by Stark effects may not be a good option as they may alter the

original electric field of the pristine air-water interface. Sum frequency generation spectroscopy (SFG) on the flat and clean air-water interface provided information about the local environment at the interface[47-49], and the observed spectral shift of the OH stretching was assigned to different types of hydrogen bonding of interfacial water.[50] Noticeably, the OH dangling bond pointing toward the vapor phase has a frequency of ~3700 cm^{-1}. This frequency can report the local electric field at the air-water interface. Since the experimental Stark tuning rate, the frequency shift in response to projected electric field along the observed chemical bond, is not yet available for the OH dangling bond vibration, the electric field cannot be determined directly from this experimental frequency.

However, molecular dynamics (MD) simulation using extended simple point charge model can help us estimate this electric field. Basically, this model establishes an empirical correlation between the observed vibrational frequencies of the OH stretching modes of water and the calculated electric field exerted at the H atom and projected along the OH bond.[51-54] This electric field was summed up from the electric field of atoms from neighboring-water molecules. This correlation, also known as the OH frequency map, is quite robust and can be applied to bulk, surface, and cluster water.[54] Using Figure 2 in Ref. 54, the corresponding electric field for the 3700 cm^{-1} vibration is about 0.01 atomic units or 50 MV/cm. SFG spectroscopy on flat water surface also detected a strong intensity in the 3400-3100 cm^{-1} region, which was assigned to the signal of water molecules residing next to the adjacent surface water molecules.[50] Using the same empirical correlation, this low frequency region corresponds to an electric field of about 200-260 MV/cm. Note that this estimation is extrapolated from measurements on flat surfaces, and we are trying to apply it to micron-sized water droplets aforementioned.

Recent MD simulations for water droplets of 8-16 nm in diameter show that the electric field at the droplet surface exhibits a Lorentzian distribution in which its center value is less than 9 MV/cm but its tail can reach to hundreds of MV/cm.[55] These electric fields were calculated at specific points on the droplet surface, and their strength is not far from the values obtained from the above vibrational frequency map. These results indicate that the water molecules at or near the interfaces can have some thermally fluctuating

arrangements that randomly produce a very high local electric field, possibly up to several hundreds of MV/cm.

Even though a local electric field up to several hundreds of MV/cm at the air-water interface seems to be a high value, it is important to know that this field strength is not surprisingly high when compared to the bulk value. The continuum solvent model estimates that the surrounding water can exert an electric field up to about 200 MV/cm on a water molecule in the bulk.[56] As liquid water has the OH stretching frequency in 3700-2800 cm^{-1} region, the corresponding electric field estimated from the frequency map method is about 0 to 300 MV/cm.[54] Apparently, these strong local electric fields do not cause H_2O_2 formation in bulk water.

Can a strong electric field shift the PES of water reaction to favor H_2O_2 product at the interface?

We anticipate that electric fields can generally influence thermodynamics and kinetics of a chemical reaction, but it is still unknown at which strength they can shift the PES of this reaction. The same MD simulations for 8-16 nm water droplets mentioned above show that the projected electric field on the OH bonds of water molecules inside the droplets has a distribution centered at 0.3 MV/cm and its width is about tens of MV/cm.[55] Note that this electric field strength is different from values obtained from the frequency map method[54] and the continuum solvent model[56] mentioned above. This difference comes from where and how the local electric field was calculated. The same MD simulations for the free OH bonds of surface water has a broad distribution centered at ~16 MV/cm and this field strength can destabilize the OH bond.[55] The tail of this distribution also can reach up to about a hundred of MV/cm. While it was not clearly confirmed that this destabilization could be sufficient to shift the PES to favor H_2O_2 product, those results suggest that the large local electric field could be a source of H_2O_2 formation. However, future work must perform a full calculation of the PES when moving from bulk to interfacial water under the effect of local electric fields. Figure 13 illustrates this approach by depicting the shift of the reaction pathway.

A recent study focuses on ionization energy of $^-$OH forming $^\bullet$OH at the air-water interface, wherein the VIEs of partially solvated $^-$OH ions are greatly lowered relative to

the average VIE of a fully solvated $^{-}$OH in the liquid phase.[41] Although this MD simulation provides an important explanation for the possible formation of OH$^{\bullet}$ due to electric field fluctuation at the droplet surfaces, a key step in H_2O_2 formation, this result is for 4-nm water droplets and quite far from a complete picture of the PES.

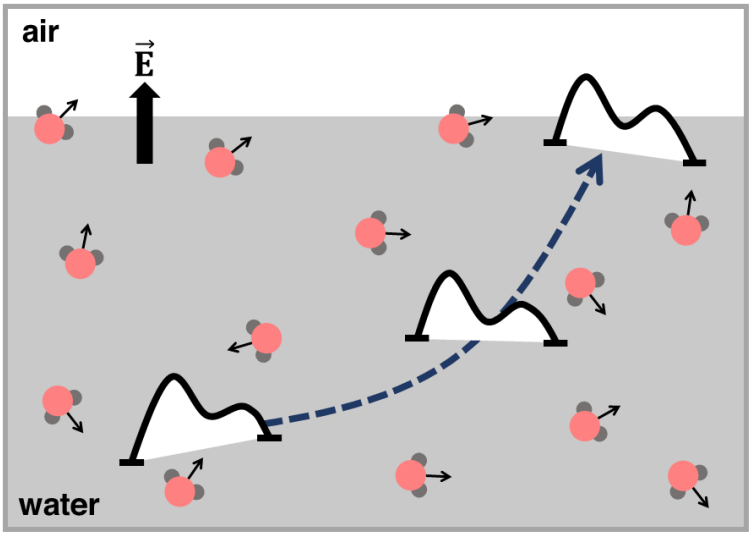

Figure 13. In order to investigate whether the $H_2O_{(l)} \rightarrow ½\ H_2O_{2(aq)} + ½\ H_{2(g)}$ reaction spontaneously occurring at the water droplet surface, the reaction pathway should be determined and projected from the bulk to the interface. The effect of local electric fields on the pathway should also be considered.

Outlook

Current research on claims of spontaneous H_2O_2 formation at the air-water interface of water droplets ultimately reflects our limited understanding of interfacial chemistry. With the quick response from our research community, new results with better control and consideration have provided more insight, but conclusions on the feasibility of these claims remain unsettled. Reporting experimental details has been critical to reproducibility and self-correction. Given their significant impact, these claims deserve further experimental confirmations and theoretical interpretation, such as detecting H_2 byproduct and determining free Gibbs energy of this interfacial reaction. We hope that the brief discussions on experimental and thermodynamic approaches presented here will inspire more researchers to participate in this intriguing research direction.

References

1. Zhong, J.; Kumar, M.; Anglada, J. M.; Martins-Costa, M. T. C.; Ruiz-Lopez, M. F.; Zeng, X. C.; Francisco, J. S., Atmospheric Spectroscopy and Photochemistry at Environmental Water Interfaces. *Annual Review of Physical Chemistry* **2019,** *70* (1), 45-69.

2. Ruiz-Lopez, M. F.; Francisco, J. S.; Martins-Costa, M. T. C.; Anglada, J. M., Molecular reactions at aqueous interfaces. *Nature Reviews Chemistry* **2020,** *4* (9), 459-475.

3. Wei, Z.; Li, Y.; Cooks, R. G.; Yan, X., Accelerated Reaction Kinetics in Microdroplets: Overview and Recent Developments. *Annual Review of Physical Chemistry* **2020,** *71* (1), 31-51.

4. Kusaka, R.; Nihonyanagi, S.; Tahara, T., The photochemical reaction of phenol becomes ultrafast at the air–water interface. *Nature Chemistry* **2021,** *13*, 306-311.

5. Deal, A. M.; Rapf, R. J.; Vaida, V., Water–Air Interfaces as Environments to Address the Water Paradox in Prebiotic Chemistry: A Physical Chemistry Perspective. *The Journal of Physical Chemistry A* **2021,** *125* (23), 4929-4942.

6. Benjamin, I., Chemical Reactions and Solvation at Liquid Interfaces: A Microscopic Perspective. *Chemical Reviews* **1996,** *96* (4), 1449-1476.

7. Jungwirth, P.; Tobias, D. J., Specific Ion Effects at the Air/Water Interface. *Chem. Rev.* **2006,** *106* (4), 1259-1281.

8. Otten, D. E.; Shaffer, P. R.; Geissler, P. L.; Saykally, R. J., Elucidating the mechanism of selective ion adsorption to the liquid water surface. *Proceedings of the National Academy of Sciences* **2012,** *109* (3), 701-705.

9. Verreault, D.; Allen, H. C., Bridging the gap between microscopic and macroscopic views of air/aqueous salt interfaces. *Chemical Physics Letters* **2013,** *586*, 1-9.

10. Lee, J. K.; Walker, K. L.; Han, H. S.; Kang, J.; Prinz, F. B.; Waymouth, R. M.; Nam, H. G.; Zare, R. N., Spontaneous generation of hydrogen peroxide from aqueous microdroplets. *Proceedings of the National Academy of Sciences* **2019,** *166* (39), 19294-19298.

11. Lee, J. K.; Han, H. S.; Chaikasetsin, S.; Marron, D. P.; Waymouth, R. M.; Prinz, F. B.; Zare, R. N., Condensing water vapor to droplets generates hydrogen peroxide. *Proceedings of the National Academy of Sciences* **2020,** *117* (49), 30934-30941.

12. Saykally, R. J., Two sides of the acid–base story. *Nature Chemistry* **2013,** *5*, 82.

13. Gallo, A.; Farinha, A. S. F.; Dinis, M.; Emwas, A.-H.; Santana, A.; Nielsen, R. J.; Goddard, W. A.; Mishra, H., The chemical reactions in electrosprays of water do not always correspond to those at the pristine air–water interface. *Chemical Science* **2019,** *10* (9), 2566-2577.

14. Beattie, J. K.; Djerdjev, A. M.; Warr, G. G., The surface of neat water is basic. *Faraday Discussions* **2009,** *141* (0), 31-39.

15. Mishra, H.; Enami, S.; Nielsen, R. J.; Stewart, L. A.; Hoffmann, M. R.; Goddard, W. A.; Colussi, A. J., Brønsted basicity of the air–water interface. *Proceedings of the National Academy of Sciences* **2012,** *109* (46), 18679-18683.

16. Petersen, P. B.; Saykally, R. J., Evidence for an Enhanced Hydronium Concentration at the Liquid Water Surface. *The Journal of Physical Chemistry B* **2005,** *109* (16), 7976-7980.

17. Levering, L. M.; Sierra-Hernández, M. R.; Allen, H. C., *J. Phys. Chem. C* **2007,** *111*, 8814.

18. Tarbuck, T.; Ota, S. T.; Richmond, G. L., *J. Am. Chem. Soc.* **2006,** *128*, 14519.

19. Tian, C.; Ji, N.; Waychunas, G. A.; Shen, Y. R., Interfacial Structures of Acidic and Basic Aqueous Solutions. *J Am Chem Soc* **2008,** *130* (39), 13033-13039.

20. Buch, V.; Milet, A.; Vácha, R.; Jungwirth, P.; Devlin, J. P., Water surface is acidic. *Proceedings of the National Academy of Sciences* **2007,** *104* (18), 7342-7347.

21. Iuchi, S.; Chen, H.; Paesani, F.; Voth, G. A., Hydrated Excess Proton at Water−Hydrophobic Interfaces. *The Journal of Physical Chemistry B* **2009,** *113* (13), 4017-4030.

22. Mamatkulov, S. I.; Allolio, C.; Netz, R. R.; Bonthuis, D. J., Orientation-Induced Adsorption of Hydrated Protons at the Air–Water Interface. *Angewandte Chemie International Edition* **2017,** *56* (50), 15846-15851.

23. Nguyen, S. C., Reactions. *C&EN Global Enterprise* **2022,** *100* (21), 3-3.

24. Peplow, M., Claims of water turning into hydrogen peroxide rekindle debate. *C&EN Global Enterprise* **2022,** *100* (19), 5-5.

25. Cozens, T.,Chemistry World, https://www.chemistryworld.com/news/study-casts-doubt-on-water-microdroplets-ability-to-spontaneously-produce-hydrogen-peroxide/4015169.article (accessed Dec 29, 2022).

26. Schwierz, N.; Lam, R. K.; Gamlieli, Z.; Tills, J. J.; Leung, A.; Geissler, P. L.; Saykally, R. J., Hydrogen and Electric Power Generation from Liquid Microjets: Design Principles for Optimizing Conversion Efficiency. *The Journal of Physical Chemistry C* **2016,** *120* (27), 14513-14521.

27. Zilch, L. W.; Maze, J. T.; Smith, J. W.; Ewing, G. E.; Jarrold, M. F., Charge Separation in the Aerodynamic Breakup of Micrometer-Sized Water Droplets. *The Journal of Physical Chemistry A* **2008,** *112* (51), 13352-13363.

28. Gallo Jr, A.; Musskopf, N. H.; Liu, X.; Yang, Z.; Petry, J.; Zhang, P.; Thoroddsen, S.; Im, H.; Mishra, H., On the formation of hydrogen peroxide in water microdroplets. *Chemical Science* **2022**.

29. Mehrgardi, M. A.; Mofidfar, M.; Zare, R. N., Sprayed Water Microdroplets Are Able to Generate Hydrogen Peroxide Spontaneously. *J Am Chem Soc* **2022,** *144* (17), 7606-7609.

30. Musskopf, N. H.; Gallo, A.; Zhang, P.; Petry, J.; Mishra, H., The Air–Water Interface of Water Microdroplets Formed by Ultrasonication or Condensation Does Not Produce H2O2. *The Journal of Physical Chemistry Letters* **2021,** *12* (46), 11422-11429.

31. Nguyen, D.; Nguyen, S. C., Revisiting the Effect of the Air–Water Interface of Ultrasonically Atomized Water Microdroplets on H2O2 Formation. *The Journal of Physical Chemistry B* **2022,** *126* (16), 3180-3185.

32. USA Environmental Protection Agency (EPA), Daily ozone concentrations in California, 2021

33. Chen, B.; Xia, Y.; He, R.; Sang, H.; Zhang, W.; Li, J.; Chen, L.; Wang, P.; Guo, S.; Yin, Y.; Hu, L.; Song, M.; Liang, Y.; Wang, Y.; Jiang, G.; Zare, R. N., Water-solid contact electrification causes hydrogen peroxide production from hydroxyl radical

recombination in sprayed microdroplets. *Proceedings of the National Academy of Sciences* **2022,** *119* (32), e2209056119.

34. Gao, D.; Jin, F.; Lee, J. K.; Zare, R. N., Aqueous microdroplets containing only ketones or aldehydes undergo Dakin and Baeyer–Villiger reactions. *Chemical Science* **2019,** *10* (48), 10974-10978.

35. Zhao, L.; Song, X.; Gong, C.; Zhang, D.; Wang, R.; Zare, R. N.; Zhang, X., Sprayed water microdroplets containing dissolved pyridine spontaneously generate pyridyl anions. *Proceedings of the National Academy of Sciences* **2022,** *119* (12), e2200991119.

36. Pullanchery, S.; Kulik, S.; Rehl, B.; Hassanali, A.; Roke, S., Charge transfer across C-H...O hydrogen bonds stabilizes oil droplets in water. *Science* **2021,** *374* (6573), 1366-1370.

37. Donaldson, D. J., Experimental Confirmation of H2O2 Adsorption at the Water–Air Interface. *The Journal of Physical Chemistry A* **2022,** *126* (33), 5647-5653.

38. Vácha, R.; Slavíček, P.; Mucha, M.; Finlayson-Pitts, B. J.; Jungwirth, P., Adsorption of Atmospherically Relevant Gases at the Air/Water Interface: Free Energy Profiles of Aqueous Solvation of N2, O2, O3, OH, H2O, HO2, and H2O2. *The Journal of Physical Chemistry A* **2004,** *108* (52), 11573-11579.

39. Martins-Costa, M. T. C.; Ruiz-López, M. F., Reaching multi-nanosecond timescales in combined QM/MM molecular dynamics simulations through parallel horsetail sampling. *Journal of Computational Chemistry* **2017,** *38* (10), 659-668.

40. Martins-Costa, M. T. C.; Anglada, J. M.; Francisco, J. S.; Ruiz-Lopez, M. F., Reactivity of Atmospherically Relevant Small Radicals at the Air–Water Interface. *Angewandte Chemie International Edition* **2012,** *51* (22), 5413-5417.

41. Heindel, J. P.; Hao, H.; LaCour, R. A.; Head-Gordon, T., Spontaneous Formation of Hydrogen Peroxide in Water Microdroplets. *The Journal of Physical Chemistry Letters* **2022,** *13*, 10035-10041.

42. Fried, S. D.; Boxer, S. G., Electric Fields and Enzyme Catalysis. *Annual Review of Biochemistry* **2017,** *86* (1), 387-415.

43. Shaik, S.; Danovich, D.; Joy, J.; Wang, Z.; Stuyver, T., Electric-Field Mediated Chemistry: Uncovering and Exploiting the Potential of (Oriented) Electric Fields to Exert Chemical Catalysis and Reaction Control. *J Am Chem Soc* **2020,** *142* (29), 12551-12562.

44. Léonard, N. G.; Dhaoui, R.; Chantarojsiri, T.; Yang, J. Y., Electric Fields in Catalysis: From Enzymes to Molecular Catalysts. *ACS Catalysis* **2021,** *11* (17), 10923-10932.

45. Che, F.; Gray, J. T.; Ha, S.; Kruse, N.; Scott, S. L.; McEwen, J.-S., Elucidating the Roles of Electric Fields in Catalysis: A Perspective. *ACS Catalysis* **2018,** *8* (6), 5153-5174.

46. Xiong, H.; Lee, J. K.; Zare, R. N.; Min, W., Strong Electric Field Observed at the Interface of Aqueous Microdroplets. *The Journal of Physical Chemistry Letters* **2020,** *11* (17), 7423-7428.

47. Du, Q.; Superfine, R.; Freysz, E.; Shen, Y. R., Vibrational spectroscopy of water at the vapor/water interface. *Physical Review Letters* **1993,** *70* (15), 2313-2316.

48. Nihonyanagi, S.; Yamaguchi, S.; Tahara, T., Direct evidence for orientational flip-flop of water molecules at charged interfaces: A heterodyne-detected vibrational sum frequency generation study. *The Journal of Chemical Physics* **2009,** *130* (20), 204704.

49. Sun, S.; Tang, F.; Imoto, S.; Moberg, D. R.; Ohto, T.; Paesani, F.; Bonn, M.; Backus, E. H. G.; Nagata, Y., Orientational Distribution of Free O-H Groups of Interfacial Water is Exponential. *Physical Review Letters* **2018,** *121* (24), 246101.

50. Scatena, L. F.; Brown, M. G.; Richmond, G. L., Water at hydrophobic surfaces: Weak hydrogen bonding and strong orientation effects. *Science* **2001,** *292* (5518), 908-912.

51. Auer, B. M.; Skinner, J. L., IR and Raman spectra of liquid water: Theory and interpretation. *The Journal of Chemical Physics* **2008,** *128* (22), 224511.

52. Niu, K.; Marcus, R. A., Sum frequency generation, calculation of absolute intensities, comparison with experiments, and two-field relaxation-based derivation. *Proceedings of the National Academy of Sciences* **2020,** *117* (6), 2805-2814.

53. Baiz, C. R.; Błasiak, B.; Bredenbeck, J.; Cho, M.; Choi, J.-H.; Corcelli, S. A.; Dijkstra, A. G.; Feng, C.-J.; Garrett-Roe, S.; Ge, N.-H.; Hanson-Heine, M. W. D.; Hirst,

J. D.; Jansen, T. L. C.; Kwac, K.; Kubarych, K. J.; Londergan, C. H.; Maekawa, H.; Reppert, M.; Saito, S.; Roy, S.; Skinner, J. L.; Stock, G.; Straub, J. E.; Thielges, M. C.; Tominaga, K.; Tokmakoff, A.; Torii, H.; Wang, L.; Webb, L. J.; Zanni, M. T., Vibrational Spectroscopic Map, Vibrational Spectroscopy, and Intermolecular Interaction. *Chemical Reviews* **2020,** *120* (15), 7152-7218.

54. Gruenbaum, S. M.; Tainter, C. J.; Shi, L.; Ni, Y.; Skinner, J. L., Robustness of Frequency, Transition Dipole, and Coupling Maps for Water Vibrational Spectroscopy. *Journal of Chemical Theory and Computation* **2013,** *9* (7), 3109-3117.

55. Hao, H.; Leven, I.; Head-Gordon, T., Can electric fields drive chemistry for an aqueous microdroplet? *Nat Commun* **2022,** *13* (1), 280.

56. Chalmet, S.; Ruiz-López, M. F., The reaction field of a water molecule in liquid water: Comparison of different quantum/classical models. *The Journal of Chemical Physics* **2001,** *115* (11), 5220-5227.

Chapter 5

Conclusions

Aqueous interfaces can be found in many chemical systems and their properties on changing kinetics and thermodynamics of chemical reactions are important for discoveries of new chemistry innovations.[1-3] The work in this thesis provides more insights into mechanism of reactions at the organic-water and the air-water interface.

In chapter 2, rate accelerations of organic reactions at the organic-water interface are investigated in great detail. Previous studies were unable to control the total interfacial area during reaction course, which prevents reliable kinetics of this phenomenon.[4] I show that by coating surfaces of mesoporous silica nanoparticles (MSNs) with a thin layer of water, I can produce a quantifiable water interfacial area for kinetic studies. The cycloaddition reaction of quadricyclane and diethyl azodicarboxylate (DEAD) at the toluene - absorbed water interface, within silica pores, was used as a model reaction. Dangling OH groups of water at the interface are proven to play a key role in catalysis. These dangling OH groups can activate DEAD as well as stabilize the transition state via hydrogen bond formation, which lowers the activation of the cycloaddition reaction. Kinetic data suggests that the reaction follows the Eley–Rideal mechanism, wherein DEAD adsorbs at the toluene–water interface via hydrogen bonds while quadricyclane diffuses to the interface and reacts with the adsorbed DEAD. Although the effects of confinement in silica pores and interfacial potential on the reaction mechanism are beyond the scope of this study, the mechanistic insights gained and preparation of surface water in silica pores described herein may facilitate the future design and applications of "on-water" catalysis.

In chapter 3, I investigate claims of spontaneous H_2O_2 formation at the air-water interface of water microdroplets. H_2O_2 is an important oxidant in the air and aqueous H_2O_2 plays an important role in atmospheric chemistry.[5] Although gas-phase H_2O_2 is mainly produced by HO_2 radical recombination, the formation of aqueous-phase H_2O_2 in troposphere is unclear.[6, 7] Therefore, the understanding of this phenomenon can advance atmospheric chemistry. A previous study proposed that the electric field at water droplet surface is the driving force of H_2O_2 formation; however, uses of an ultrasonic humidifier to generate those water droplets face a potential for contamination.[8] In this dissertation, effects of water droplet formation and the electric field at the droplet surface on these H_2O_2 observations were first revisited in chapter 4. When tuning the electric field by adsorption

of ionic surfactants at droplet surfaces, H_2O_2 formation does not change. In contrast, water sonolysis due to ultrasound shows a strong correlation with H_2O_2 production. Thus, it is expected that the observation of H_2O_2 in the previous study could be due to experimental artifacts. Then, more experimental and thermodynamic considerations on these H_2O_2 observations were discussed in detail in chapter 5.

Overall, chemistry at aqueous interfaces shows interesting properties, yet collecting experimental evidence is a challenging task. Future work should focus on using different approaches and experimental techniques to reliably study chemical reactions, thus driving more explorations in the field of chemistry at the interface.

Reference

1. Ruiz-Lopez, M. F.; Francisco, J. S.; Martins-Costa, M. T. C.; Anglada, J. M., Molecular reactions at aqueous interfaces. *Nat Rev Chem* **2020,** *4* (9), 459-475.

2. Benjamin, I., Chemical Reactions and Solvation at Liquid Interfaces: A Microscopic Perspective. *Chemical Reviews* **1996,** *96* (4), 1449-1476.

3. Geiger, F. M., A Virtual Issue on Aqueous Interfaces. *J Phys Chem B* **2021,** *125* (37), 10401-10403.

4. Narayan, S.; Muldoon, J.; Finn, M. G.; Fokin, V. V.; Kolb, H. C.; Sharpless, K. B., "On water": unique reactivity of organic compounds in aqueous suspension. *Angew Chem Int Ed Engl* **2005,** *44* (21), 3275-9.

5. Vione, D.; Maurino, V.; Minero, C.; Pelizzetti, E., The atmospheric chemistry of hydrogen peroxide: A review. *Ann Chim-Rome* **2003,** *93* (4), 477-488.

6. Moller, D., Atmospheric hydrogen peroxide: Evidence for aqueous-phase formation from a historic perspective and a one-year measurement campaign. *Atmos Environ* **2009,** *43* (37), 5923-5936.

7. Zhu, C. Q.; Francisco, J. S., Production of hydrogen peroxide enabled by microdroplets. *P Natl Acad Sci USA* **2019,** *116* (39), 19222-19224.

8. Lee, J. K.; Han, H. S.; Chaikasetsin, S.; Marron, D. P.; Waymouth, R. M.; Prinz, F. B.; Zare, R. N., Condensing water vapor to droplets generates hydrogen peroxide. *P Natl Acad Sci USA* **2020,** *117* (49), 30934-30941.

Appendix

Appendix A

Preparation of dry silica nanoparticles

Preparation of nonporous silica nanoparticles. Nonporous silica nanoparticles were synthesized by Stöber method.[1] Tetraethyl orthosilicate (TEOS, 10 mL) was quickly injected into a mixture of H_2O (44 mL), 2-propanol (196 mL), and ammonia solution 28 – 30 % (20 mL) at room temperature and under stirring. After 3 hours of reaction, the particles were collected by centrifugation (16,639 g-force, 10 min), washed 3 times with water, and then heated overnight at 120 ^oC. The dry particles were then stored in vials sealed with Parafilm.

Preparation of mesoporous silica nanoparticles. Mesoporous silica nanoparticles with highly ordered hexagonal pore array were synthesized using modified Stöber method with the addition of hexadecyltrimethylammonium chloride (CTAC) as a structure-directing agent.[2] This method produces porous particles with good size distribution, uniform spherical shape and less surface defects as compared other porous silica particles, such as SBA-15 or MCM-41.[3] This condition is important for determining precisely the silica surface and adsorbed water for kinetic study. Particle sizes can be tuned by increasing the methanol/water ratio for larger sizes.[2] For a typical procedure of preparing particles of 542 nm diameter, 3.44 g of CTAC was dissolved in a mixture of water (400 g) and methanol (400 g). Then, 2.30 mL of NaOH 1.0 M was added to the solution under stirring. Then, 1.30 mL of tetramethyl orthosilicate (TMOS) was quickly injected under vigorous stirring. The mixture was stirred for another 8 hours, and then aged overnight at room temperature. The obtained particles were collected by centrifugation (16,639 g-force, 15 min), washed with methanol and water 3 times, and subsequently dried at 50 ^oC for a day. Afterward, the CTAC was removed by calcinating the particles at 550 ^oC for 6 hrs. The particles were then stored in vials sealed with Parafilm.

Preparation of water-adsorbed silica nanoparticles

Preparation of water-adsorbed silica nanoparticles for kinetic studies and SHS experiments: Dry silica nanoparticles were let to adsorb water vapor in a home-built box at room temperature. The box was sealed to build up saturated water vapor at room

temperature and the dry nanoparticles adsorbed vaporized water for a certain amount of time. The box was placed in a low power ultrasonic bath to promote mechanical agitation that ensured the adsorbed water was dispersed evenly inside the particles. The amount of adsorbed water was controlled by the period of the particles staying in the box and determined by FTIR spectroscopy. The adsorbed water reached a plateau under 1 hour sonication, and there were about 4 water molecules per 1 nm^2 of silica surface in the porous particles.

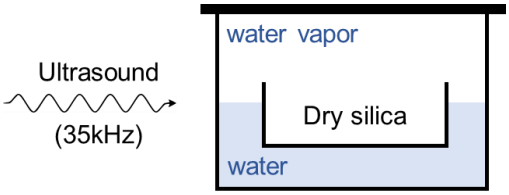

Scheme A1. The home-built humidity-controlled box for controlling water adsorbed on porous and non-prorous silica nanoparticles.

Preparation of water-adsorbed silica nanoparticles for studying kinetic isotope effects: We first tried the above method to load D_2O on silica nanoparticles; however, there was a significant amount of pre-existed H_2O in the air that co-adsorbed on the particles. To mitigate this problem, we placed the box in an oven at 35 ^oC for 6 hours to promote the evaporation of D_2O (Scheme A2). To ensure that D_2O adsorbed evenly onto silica, the sample was stirred in the middle of the adsorption process. Eventually, the majority of adsorbed water is D_2O. FTIR spectroscopy confirmed that 85% of adsorbed water on silica nanoparticles was D_2O (Figure A4). A reference sample was prepared with H_2O under the same adsorption process for comparing the kinetic isotope effect.

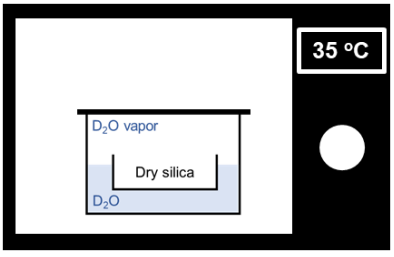

Scheme A2. The home-built enclosed box for controlling D_2O (or H_2O) adsorbed on porous silica nanoparticles for studying kinetic isotope effects.

Determination of surface water molecules adsorbed in mesoporous silica nanoparticles via FTIR spectroscopy

Spectroscopic characterization of surface water adsorbed in silica pores: An amount of 2 mg mesoporous silica particles was mixed with 40 mg spectroscopic grade KBr, then pressed into a pellet (diameter of 7 mm and thickness of ~ 1 mm) for FTIR measurement. The result was reported in Figure A1.

Quantification of water adsorbed in silica pores: The total amount of adsorbed water was quantified by the peak area of the HOH bending mode at 1627 cm^{-1}. In order to use the absorption coefficient value of the HOH bending mode from a previous experiment,[4] we avoided using KBr matrix. In fact, dry mesoporous silica nanoparticles were used as a matrix to achieve the same experimental condition as reported in the previous study. In our experiment, each water adsorbed-silica nanoparticle sample was mixed with the dried version (5.0 mg, served as a matrix) and pressed into a pellet for FTIR measurement. The following formula was used to calculate the amount of adsorbed water since the IR beam covers the entire base area S of the pellet.

$$A_{H_2O} = \varepsilon_{H_2O}.l.C_{H_2O}$$

$$A_{H_2O} = \varepsilon_{H_2O}.l.\frac{n_{H_2O}}{\pi r^2 l}$$

$$A_{H_2O} = \varepsilon_{H_2O}.\frac{n_{H_2O}}{S}$$

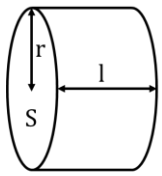

Silica pellet

where:

A_{H_2O}(cm^{-1}): peak area of the HOH bending mode.

ε_{H_2O} ($cm.\mu mol^{-1}$) = 1.53 ± 0.03, which is the integrated molar absorption coefficient from a previous study.[4]

n_{H_2O}(μmol): mole of water

S(cm^2) = $\pi r^2 = \pi \times (0.35)^2$, which is the base area of the pellet.

According the original work on preparing these mesoporous silica nanoparticles,[2] the particles have specific surface area of 1155 $m^2.g^{-1}$ and pore volume of 0.68 $cm^3.g^{-1}$. These values were used to calculate the average percentage mass of water in silica nanoparticles, the average percentage volume of water occupied the particle pore and the average water molecules per nm^2 of silica surface. The results were reported in Figure 6b and Table A1.

Typical reaction condition for "on-water" catalysis

Generally, the 2 mL-vial containing DEAD 40% in toluene (546 μL, 1.87 M) and silica nanoparticle catalyst (11 % w/w) was sonicated for 1 min to disperse the particles. Then, quadricyclane (94 μL, 1.57 M) was added. The reaction mixture was stirred at room temperature for 24 hours and the particles dispersed well during the reaction. After reaction completion, the catalyst was removed by centrifugation (14,100 g-force, 5 min) and the supernatant was used as the crude reaction mixture for ^{1}H NMR analysis. All experiments were repeated multiple times to get experimental uncertainties which are reported as one standard deviation of the means.

Determination of initial reaction rate

The initial reaction rates were determined by observing the DEAD concentration within less than 10 % reaction conversion via UV-Vis spectroscopy. The absorbance of DEAD (at λ_{max} = 405 nm) is well separated from those of quadricyclane, reaction product and toluene solvent. During the reaction, a certain amount of reaction mixture was extracted at a particular time, then diluted by cold toluene (10 ^{o}C) to quench the reaction (Table A3). The solution was then centrifuged (14,100 g-force, 5 min) to remove silica particles, and the concentration of DEAD was determined by UV-vis spectroscopy and scaled by the above dilution. The extinction coefficient of DEAD is 51.89 L.mol^{-1}.cm^{-1}, which was obtained from our standard curve. The initial reaction rate was determined from the slope of a linear regression of DEAD concentration versus reaction time. As mentioned in the main text, the initial rate of the catalyzed reaction was corrected by subtracting the initial rate of non-catalyzed reaction within similar experimental condition.

The Gibbs free energy of adsorption of DEAD on the water adsorbed mesoporous silica nanoparticles

Second harmonic scattering (SHS) spectroscopy: The angle-resolved second harmonic spectroscopy was described elsewhere.[5, 6] The 800 nm laser pulses with an average 100 fs duration are directed through an 800-nm bandpass filter and an 800-nm λ/2 plate to obtain the desired input polarization. The laser beam is then focused through an

objective lens into the sample vial. The output second harmonic light is collected at the desired angle and polarization, spectrally filtered, then directed into a spectrograph with a PMT operated in photon counting mode. The data collection was performed in LabVIEW and data analysis were performed in Python. The raw SHS intensities were subtracted by the scattering of the optics and normalized to the scattering of toluene solvent.

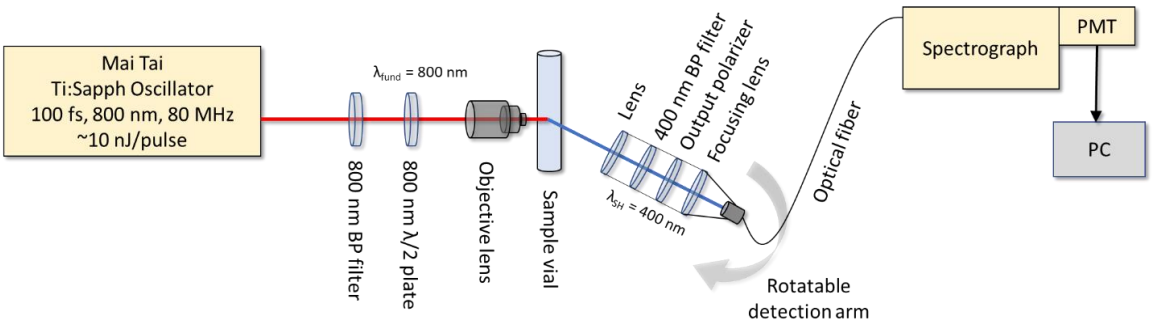

Scheme A3. The second harmonic scattering optical setup.

Experimental condition: Samples contained ~0.01 % w/w water-adsorbed or dry mesoporous silica nanoparticles (size of 430 nm) and DEAD (concentration range of 0 - 40μM) in toluene. Due to the low dispersion of the particles in the solution, the samples were sonicated for at least 10 minutes prior to SHS measurements. Each sample was collected for 3 minutes under XX-polarization (X-in, X-out) condition.

Data analysis: The SHS data were fit to a modified Langmuir adsorption isotherm model:

$$I_{SHS} = B + \left[b + a \times \theta_D \times e^{i\phi}\right]^2$$

Where B is the constant corresponded to non-resonant background scattering, b is the bulk contribution from the sample, a is a fit constant describing the signal from DEAD molecules at the interface of toluene and water, θ_D is the fractional coverage of DEAD, and ϕ is a phase factor corresponding to the interference between the particle signal and the DEAD signal. All constants in the above equation are unitless because the SHS intensity is normalized and unitless. This modified Langmuir adsorption isotherm is a typical first-order model, adjusted to account for the decrease in bulk DEAD concentration due to adsorption to the surface.

The fractional coverage is given by:

$$\theta_D = \frac{\left(C_D + N_m^D + \frac{9.44}{K_D}\right) - \sqrt{\left(C_D + N_m^D + \frac{9.44}{K_D}\right)^2 - 4C_D N_m^D}}{2N_m^D}$$

Where C_D is the total concentration of DEAD molecule in mol.L^{-1}, N_m^D is the maximum surface density of DEAD molecule in mol.L^{-1}, 9.44 M is the concentration of neat toluene, and K_D is the equilibrium constant for adsorption of DEAD on the surface water on the silica pores, given by the equilibrium:

$$\mathrm{DEAD}_{(in\ toluene\ solution)} + \mathrm{toluene} \cdot \mathrm{suface\ water} \rightleftharpoons \mathrm{toluene} + \mathrm{DEAD} \cdot \mathrm{surface\ water}$$

To calculate the Gibbs free energy of the adsorption, $\Delta G°_{ads}$, we use the following equation for a temperature of 25°C.

$$\Delta G° = -RT \ln K° = -RT \ln(9.44\ K_D)$$

Figures

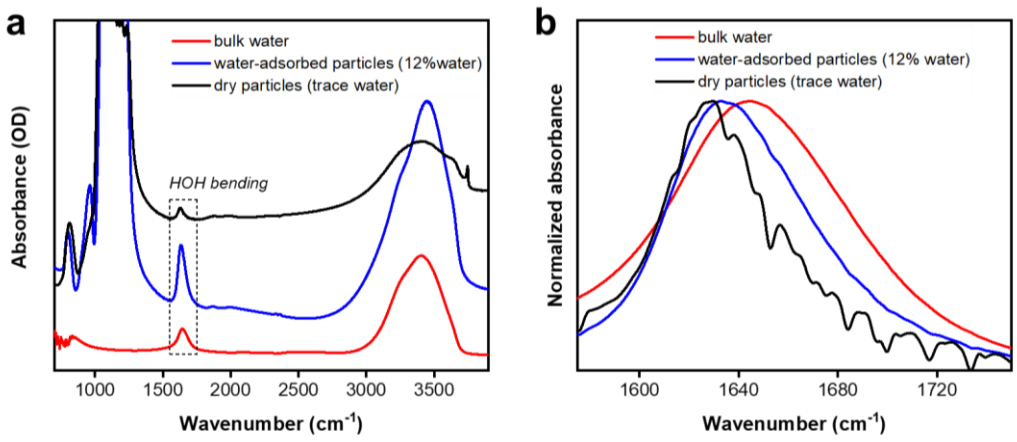

Figure A1. a) FTIR spectra of bulk water, water-adsorbed mesoporous silica nanoparticles (diameter of 542 ± 23 nm), and dry mesoporous silica nanoparticles (diameter of 542 ± 23 nm). b) Normalized absorbance of HOH bending peak from (a).

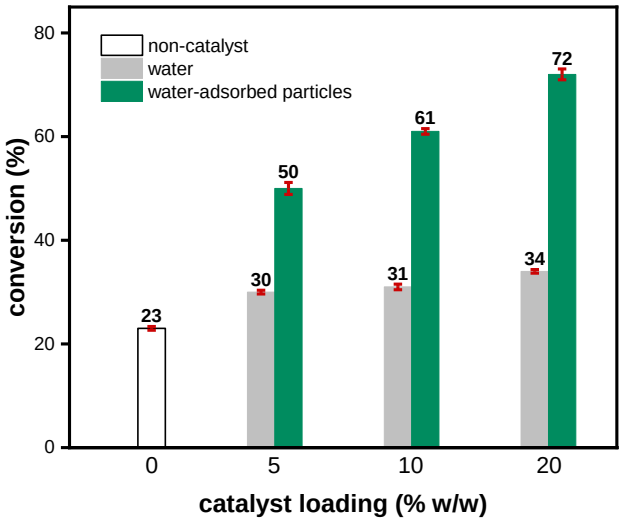

Figure A2. Comparison of catalytic activity of pure water droplets and water-adsorbed mesoporous silica nanoparticles. The diameter of the silica particles is 360 ± 56 nm. Reaction conditions: quadricyclane (100 μL), DEAD 40% in toluene (490 μL), and the catalyst under stirring. The sizes of the water droplets are unknown.

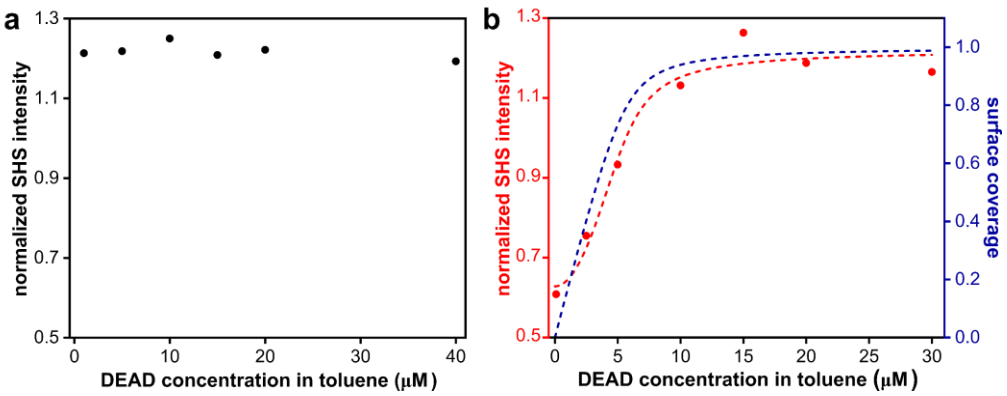

Figure A3. Measured SHS signal versus bulk DEAD concentration. a) when using dry porous silica nanoparticles (size of 430 nm); b) when using water-adsorbed porous silica nanoparticles (size of 430 nm). The experimental data were fitted to a modified Langmuir adsorption model described above. The extracted equilibrium constant (K_D) for adsorption of DEAD on surface water (or toluene-water interface) in the silica pores is 30.9 with the percentage error of 182%, the estimated $\Delta G°_{ads}$ is -3.4 kcal/mol with the propagated error of 32%. Due to the limitation of experimental points and the simplicity of the fitting model,

the $\Delta G°_{ads}$ has a larger error and was not used in our mechanistic interpretation. However, the isotherm follows a Langmuir model, and this information was used in the main text.

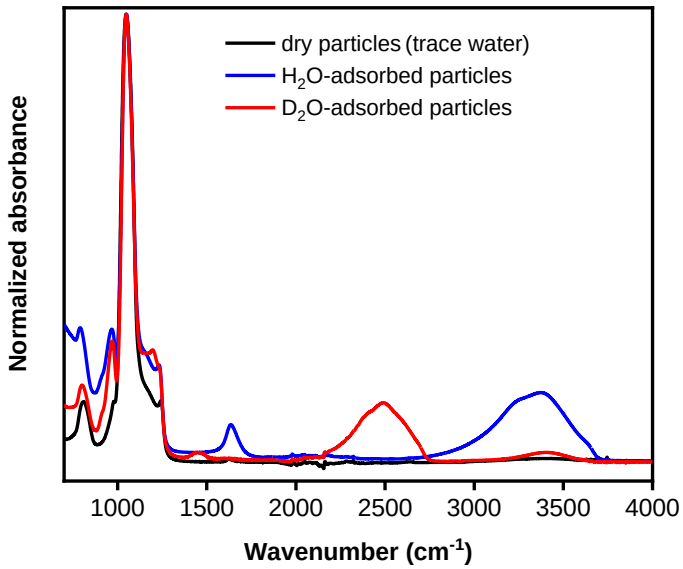

Figure A4. FTIR spectra of dry mesoporous silica nanoparticles (size of 568 ± 25 nm), the 100% pure H_2O adsorbed version of the same particles, and the 85% D_2O/15% H_2O version. All spectra are normalized to Si-O stretching vibration of silica at 1049 cm^{-1}. See sample preparation above.

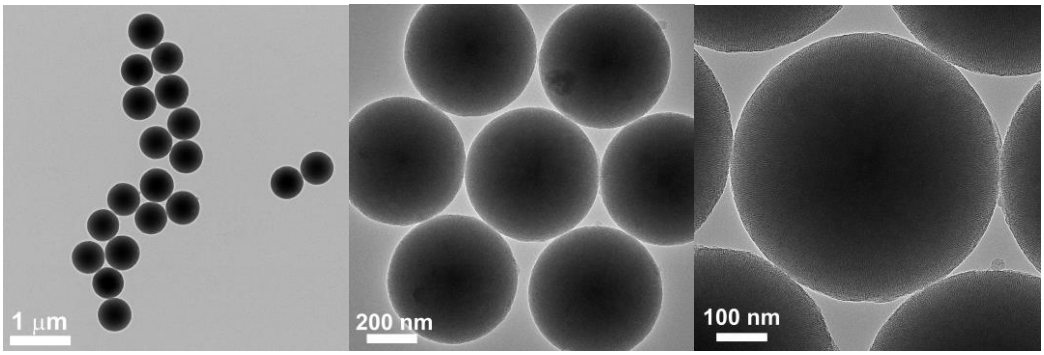

Figure A5. Reprentative TEM images show the perfect spherical shape of 597 nm mesoporous silica nanoparticles as an example for the high uniform of the studied catalysts.

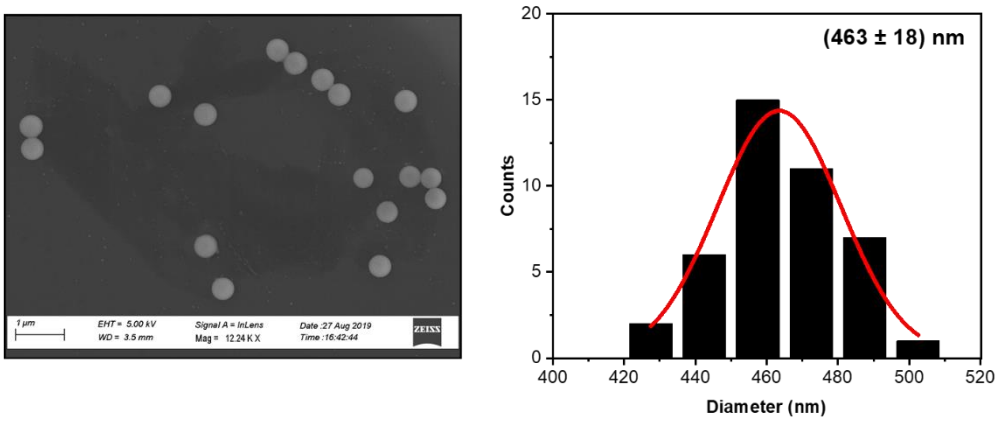

Figure A6. SEM image and the size distribution with a Gaussian distribution fitting of 463 nm non-porous silica nanoparticles.

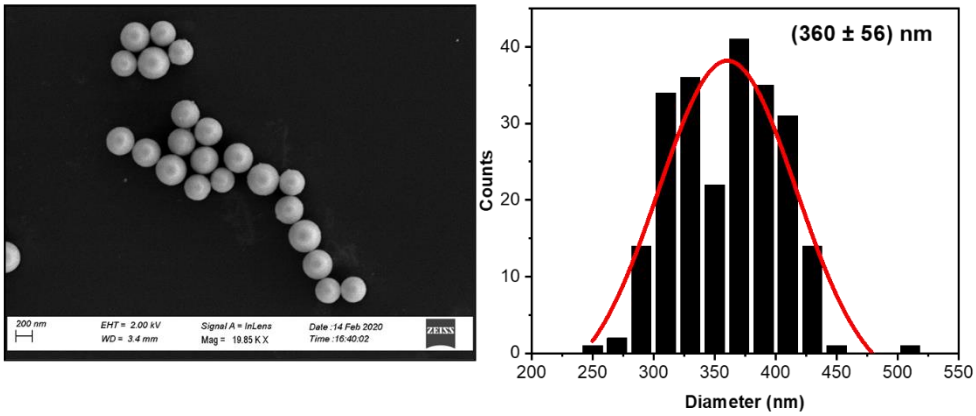

Figure A7. SEM image and the size distribution with a Gaussian distribution fitting of 360 nm mesoporous silica nanoparticles

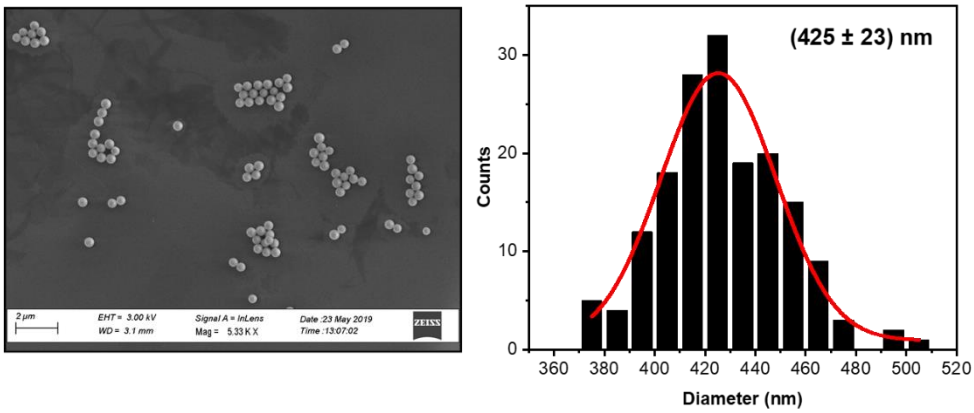

Figure A8. SEM image and the size distribution with a Gaussian distribution fitting of 425 nm mesoporous silica nanoparticles.

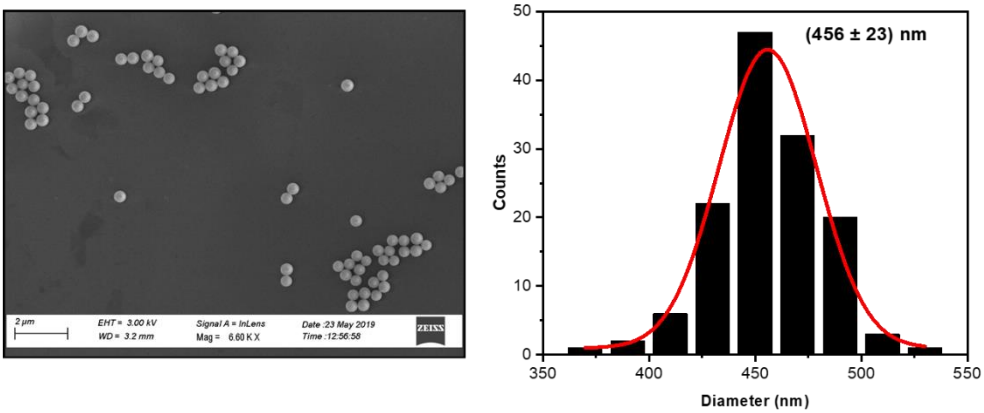

Figure A9. SEM image and the size distribution with a Gaussian distribution fitting of 456 nm mesoporous silica nanoparticles.

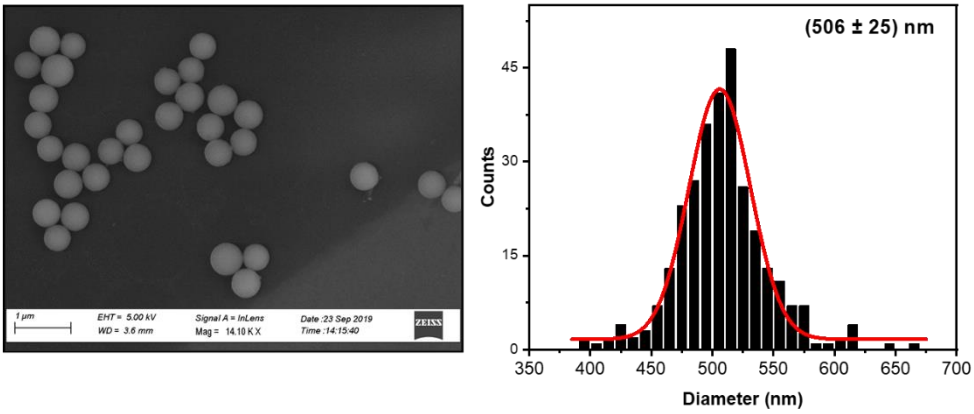

Figure A10. SEM image and the size distribution with a Gaussian distribution fitting of 506 nm mesoporous silica nanoparticles.

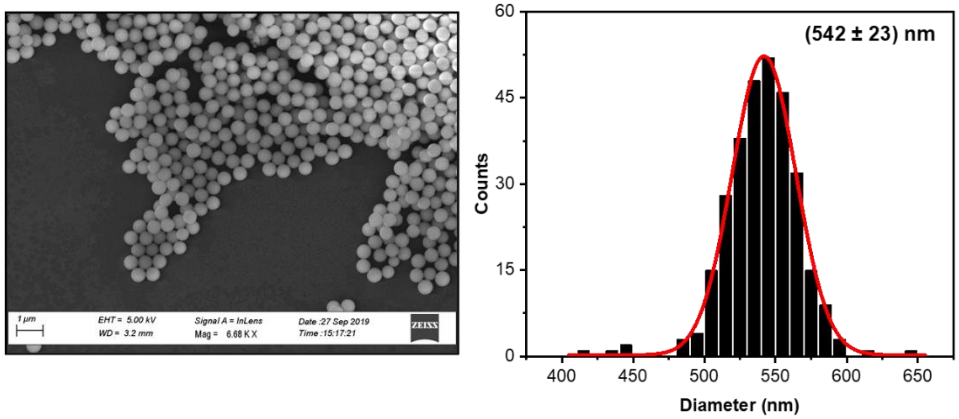

Figure A11. SEM image and the size distribution with a Gaussian distribution fitting of 542 nm mesoporous silica nanoparticles.

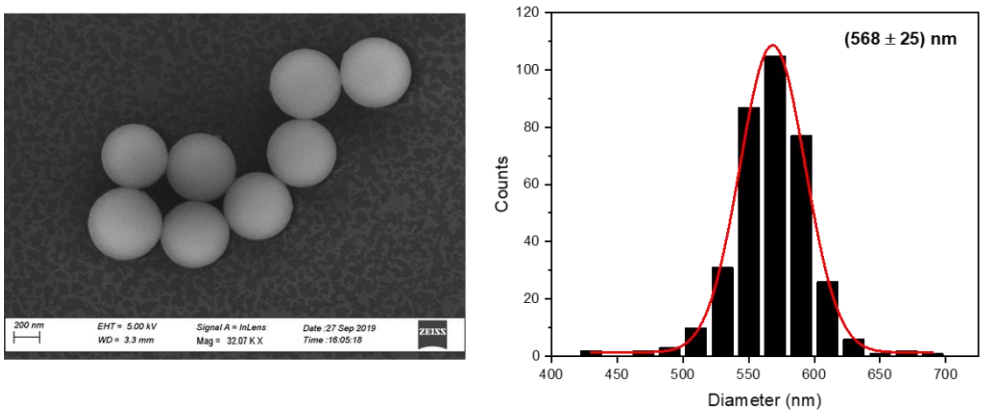

Figure A12. SEM image and the size distribution with a Gaussian distribution fitting of 568 nm mesoporous silica nanoparticles.

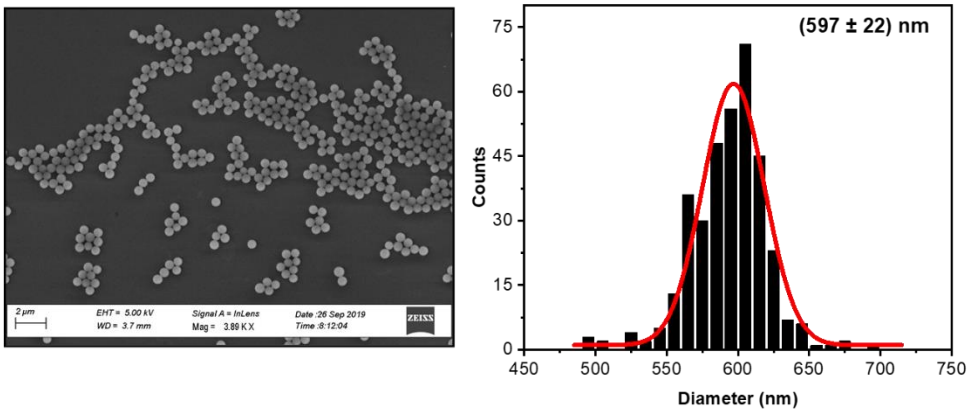

Figure A13. SEM image and the size distribution with a Gaussian distribution fitting of 597 nm mesoporous silica particles.

Tables

Table A1. Quantification of surface water molecules per nm^2 surface silica in mesoporous silica nanoparticles (see experimental details mentioned above).

Entry	Particle diameter (nm)	$\frac{m_{H_2O}}{m_{particle}}$ (%)	$\frac{v_{H_2O}}{v_{particle\ pore}}$ (%)	#H_2O/nm^2 (molecules)
1	542 ± 23	11.8 ± 1.2	20.1 ± 2.3	4.0 ± 0.5

2	506 ± 25	12.5 ± 1.6	21.4 ± 3.1	4.2 ± 0.6
3	597 ± 22	11.7 ± 1.1	19.0 ± 2.1	4.0 ± 0.4
4	425 ± 23	1.2 ± 0.1	1.8 ± 0.1	0.4 ± 0.02
5	425 ± 23	3.5 ± 0.6	5.4 ± 1.0	1.1 ± 0.2
6	425 ± 23	6.1 ± 1.5	9.7 ± 2.7	1.9 ± 0.5
7	425 ± 23	8.7 ± 0.3	14.0 ± 0.5	2.8 ± 0.1
8	425 ± 23	12.2 ± 1.1	20.6 ± 2.2	4.1 ± 0.4

Table A2. Calculated total surface areas of various silica nanoparticle catalyst in this study.

Entry	10 mg of silica nanoparticle samples		Total external surface area (cm^2)	Total internal surface area (cm^2)	Ratio of total internal surface area over total external surface area	Conversion [a] (%)
1	Dry	nonporous 463 nm	563	N/A	N/A	2
2		porous 360 nm	1858	113642	61	15
3		porous 456 nm	1467	114033	78	14
4		porous 597 nm	1120	114379	102	23
5	Water adsorbed	nonporous 463 nm	563	N/A	N/A	9
6		porous 360 nm	1771	99869	56	43
7		porous 456 nm	1398	100241	72	36
8		porous 597 nm	1068	100572	94	41

[a] after subtracting the conversion of the background reaction.

The total external surface areas were calculated from the total numbers of particles in the reaction solution and the assumption that each particle has a full surface area of a sphere. The total internal surface areas were calculated by subtracting the total external surface areas from the total surface areas. The total surface areas of the porous samples were calculated from the mass of porous silica nanoparticles and the specific surface area (about 1155m^2/g) from a previous study.[2]

Table A3. Reaction condition of kinetic studies using water-adsorbed mesoporous silica nanoparticle catalyst.

Entry	Experiment	Quadricyclane concentration in toluene (M)	DEAD concentration in toluene (M)	Porous silica nanoparticle catalyst		Temp. (°C)	Extracted volume (μL)
				Mass (mg)	Diameter (nm)		
1	Activation energy	1.57	1.87	20.0	542 ± 23	24	50
2		1.57	1.87	20.0		39	50
3		1.57	1.87	20.0		50	50
4		1.57	1.87	20.0		60	50
5	Reaction order in quadricyclane	0.84	1.00	20.0	506 ± 25	24	100
6		1.67	1.00	20.0		24	100
7		2.51	1.00	20.0		24	100
8		3.34	1.00	20.0		24	100
9	Reaction order in DEAD	1.20	0.24	15.0	542 ± 23	24	200
10		1.20	0.48	15.0		24	200
11		1.20	0.72	15.0		24	150
12		1.20	0.96	15.0		24	100
13	Reaction order in catalyst sites	1.57	1.87	5.0	597 ± 22	24	50
14		1.57	1.87	10.0		24	50
15		1.57	1.87	15.0		24	50
16		1.57	1.87	20.0		24	50

Since a large amount of mesoporous silica nanoparticles was used in our experiment, it was impossible to prepare one particle size by one large batch for all kinetic studies. Instead, particles with a bit variation in size were conveniently used for each set of experiments as showed in the table. As we proved in the main text, particles size has no

effect on the catalytic activity, thus the above size variation does not affect the mechanistic interpretation.

References

1. Stober, W.; Fink, A.; Bohn, E., Controlled Growth of Monodisperse Silica Spheres in Micron Size Range. *J Colloid Interf Sci* **1968,** *26* (1), 62-69.

2. Yano, K.; Fukushima, Y., Synthesis of mono-dispersed mesoporous silica spheres with highly ordered hexagonal regularity using conventional alkyltrimethylammonium halide as a surfactant. *J Mater Chem* **2004,** *14* (10), 1579-1584.

3. Grunberg, B.; Emmler, T.; Gedat, E.; Shenderovich, I.; Findenegg, G. H.; Limbach, H. H.; Buntkowsky, G., Hydrogen bonding of water confined in mesoporous silica MCM-41 and SBA-15 studied by 1H solid-state NMR. *Chemistry* **2004,** *10* (22), 5689-96.

4. Gallas, J.-P.; Goupil, J.-M.; Vimont, A.; Lavalley, J.-C.; Gil, B.; Gilson, J.-P.; Miserque, O., Quantification of Water and Silanol Species on Various Silicas by Coupling IR Spectroscopy and in-Situ Thermogravimetry. *Langmuir* **2009,** *25* (10), 5825-5834.

5. Cole, W. T. S.; Wei, H. Y.; Nguyen, S. C.; Harris, C. B.; Miller, D. J.; Saykally, R. J., Dynamics of Micropollutant Adsorption to Polystyrene Surfaces Probed by Angle-Resolved Second Harmonic Scattering. *J Phys Chem C* **2019,** *123* (23), 14362-14369.

6. Wang, H. F.; Yan, E. C. Y.; Liu, Y.; Eisenthal, K. B., Energetics and population of molecules at microscopic liquid and solid surfaces. *J Phys Chem B* **1998,** *102* (23), 4446-4450.

Appendix B

Chemicals and instruments

Peroxide test strips, LaMotte™ dissolved oxygen kit, and Amplex® red reagent was purchased from Thermo Fisher Scientific. Potassium titanium oxide oxalate ($K_2TiO(C_2O_4).2H_2O$, PTO), potassium chloride, sodium hydroxide, and chloric acid, and concentrated sulfuric acid, triton X-100 ($C_{34}H_{62}O_{11}$), cetyltrimethylammonium chloride (CTAC), sodium dodecyl sulfate (SDS) were purchased from Sigma-Aldrich. All samples were prepared using milli-Q water.

Ultrasonic transducer (1.7 MHz, 12 W, 400 mL H_2O/h), with the transducer disk of 1.5 cm in diameter, was purchased from AGPTEK (Amazon). The size of water droplets was measured by a BXFM optical microscope (Olympus) equipped with a EP50 camera and further analyzed by ImageJ software. Plastic tubes were obtained by modifying polypropylene barrels of 30-mL Luer-slip syringes (2.5 cm in diameter, 0.1 cm thickness, Thermo Scientific). Determination of H_2O_2 concentration by PTO and Amplex® red reagent titration was performed on a USB 4000 UV-vis spectrometer (Ocean Optics) and a CLARIOstar microplate reader (BMG Labtech), respectively.

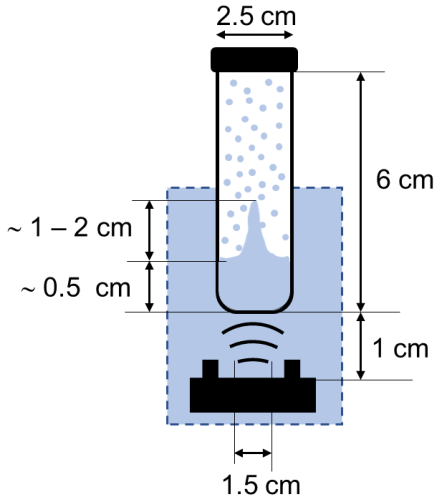

Scheme A4. Scheme of a typical experiment.

We used a commercial ultrasonic mist maker (1.7 MHz, 12 W) as a source of ultrasound to generate water droplets. We want to clarify that the humidifiers used in previous works[1, 2] and the mist makers used in this work have similar ultrasonic transducers for generating

water droplets, but the humidifiers allow the droplets to evaporate to control humidity. However, the “ultrasonic humidifier” and “ultrasonic mist maker” names are usually used interchangeably. To avoid contaminations from air-borne chemicals[3] or the transducer heads, chemical resistance polypropylene tubes containing mili-Q water, sealed by septa, were used as containers for droplet generation (Figure 6a, sample A). As MHz ultrasound from the transducer propagated through the tube, it continuously created numerous water droplets inside the tubes. When different surfactant solutions were irradiated instead of pure water, these droplets should contain the surfactants, which should change their surface properties.

In a typical experiment (Figure 6a, sample A), a sealed tube containing 3 mL of water was placed at 1 cm above the ceramic disc of the ultrasonic transducer, which was immersed in a 2.5 L water bath (see Figure 6a, Scheme A4). During ultrasonic irradiation, a protuberance (around 1−2 cm height) was formed at the water surface, and water droplets were injected from the protuberance. Each droplet had a lifetime of few seconds before it fell back into the solution. The tube underwent ultrasonic irradiation for 6 h, allowing sufficient accumulation of H_2O_2 for accurate analysis. Finally, the aliquot from the tube was directly analyzed by peroxide test strips and titration with potassium titanium oxide oxalate (PTO). We noticed that the temperature of the water in the tube rose from room temperature to about 34 °C within 3 min, and then, the water bath kept the sample at that temperature for the rest of the experiment. A 1.28 W acoustic power dissipated into the reaction solution was measured by the calorimetry method (Figure A17). In the control sample, sample B in Figure 6a, a polyethylene stopper was placed at the water surface to prevent the formation of the protuberance and water droplets. Sample B was irradiated by the same ultrasound source for 6 h. Due to a low concentration detected in the tube, the amount of H_2O_2 was then quantified by titration with Amplex red reagent (see Figure A16). To vary the amount of dissolved oxygen in water in other typical samples (as reported in Figure 7b), the tubes containing 3 mL of water were sealed by septa and purged with either N_2 or O_2 gas for 30 min. Then, the amount of dissolved oxygen in the water was measured by a LaMotte dissolved oxygen kit (see results in Table A4).

Hydrogen peroxide characterization

Peroxide test strip: 10 μL of the ultrasonic-irradiated solution was pipetted on a peroxide test strip. The detection range of the test strip is 14.7 – 735 μM. Due to the poor quantification of this method, we did not report the actual concentration of H_2O_2, however the test strips did detect H_2O_2.

Titration with potassium titanium oxide oxalate (PTO): 1.0 mL of the ultrasonic-irradiated solution and 1.0 mL of stock PTO solution were added into a quartz cuvette for UV-vis spectroscopy. The absorbance at 398 nm of titanium(IV)-peroxide complex product was used to build the standard curve for quantifying [H_2O_2] (Figure A15). The detection limit is about 10 μM H_2O_2.[4]

Stock PTO solution was prepared by mixing 28.4 mL of water, 1.6 mL of 98% H_2SO_4, and 0.21 g of PTO.

Amplex® red hydrogen peroxide/peroxidase assay kit: 50 μL of Amplex® red reagent solution was added into microplate wells, each containing 50 μL of analyzed sample, and incubated for 30 minutes before fluorescence measurements (530 nm excitation, 590 nm fluorescence detection). Background correction for fluorescence detection was done on the similar sample without H_2O_2. Figure S3 shows the standard curve for quantifying [H_2O_2]. As given by the manufactory, the detection limit of this assay is 0.1 μM H_2O_2. We only used this method to analyze sample B reported in Figure 6 since the H_2O_2 concentration was low.

Acoustic power measurement

The power dissipated to the solution inside the plastic tube was determined by calorimetry method, assuming that all ultrasonic energy delivered to the solution is dissipated as heat:[5]

$$P_{diss} = (\frac{dT}{dt})_{t=0} mC_p = 1.28\ (W)$$

where m (kg) = 3.0×10^{-3} as mass of water,

C_p ($J.K^{-1}.kg^{-1}$) = 4184 as heat capacity of water,

$(\frac{dT}{dt})_{t=0}$ (K.s^{-1}) = 1.02 as the initial slope of the water's temperature rise versus time of ultrasound exposure. As shown in Figure A17, the slope was extracted at the early time of irradiation to minimize the heat dissipation out of the tube.

Droplet size measurement

We measured the size of droplets generated from a typical sample, such as sample A in Figure 6. During ultrasonic irradiation, the tube was opened and allowed the water droplets land onto a microscope calibration slide (Figure A1). The BXFM optical microscope equipped with the EP50 camera recorded the landed droplets. The frames at instant landing were analyzed to get the closet value of the actual droplet size. ImageJ was used to extract the size from these frames, and a Gaussian distribution of 7.2 ± 3.3 μm was fitted well to most of the measured size. This droplet size is in good agreement with the size measured by laser diffraction method (6.71 ± 1.83 μm) in a previous work where an ultrasonic mist maker was used in similar way.[6] Note that there are many large droplets (size >12 μm) on the slide probably due to coalescence of droplets.

Figures

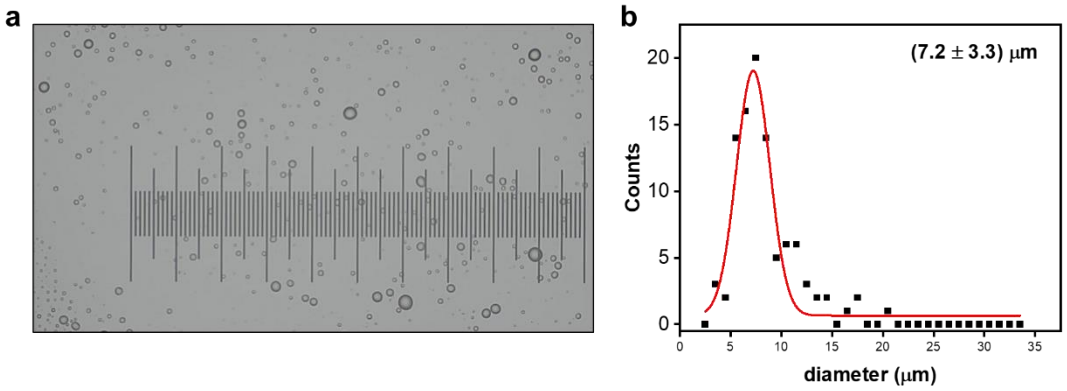

Figure A14. (a) An image captured by the BXFM optical microscope, (b) size distribution (Gaussian distribution fitting) of water droplets. Scale: 1 Div. = 10 μm.

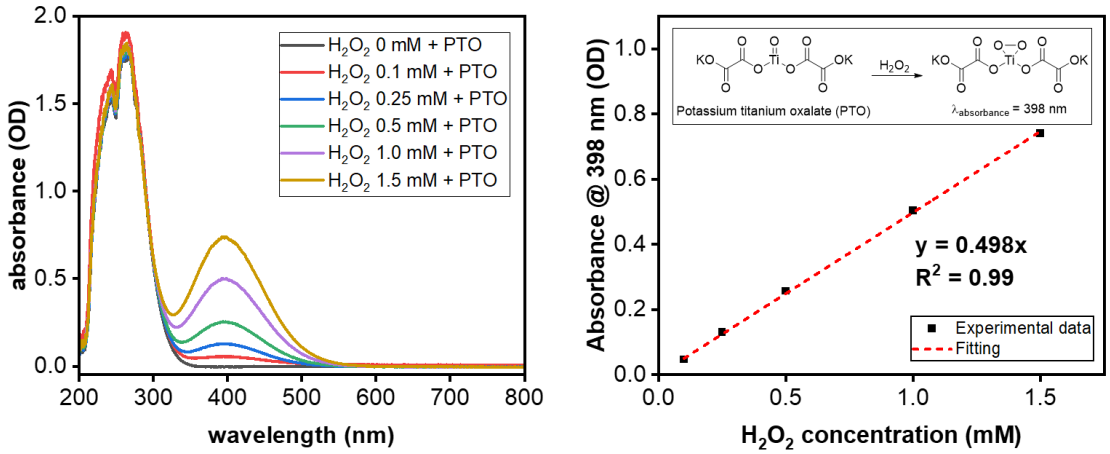

Figure A15. (a) UV–vis spectra of aqueous mixtures of PTO and H_2O_2. (b) Standard curve for H_2O_2 quantification by titration with PTO.

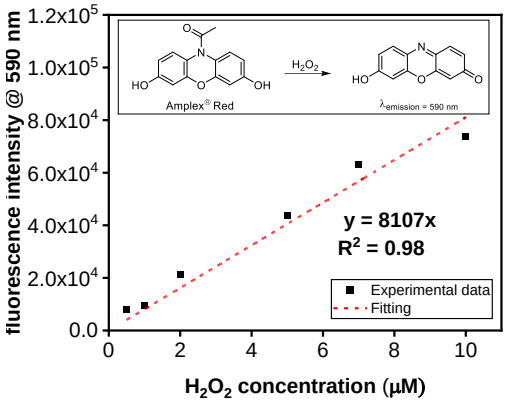

Figure A16. Standard curve for H_2O_2 quantification by titration with Amplex® red reagent.

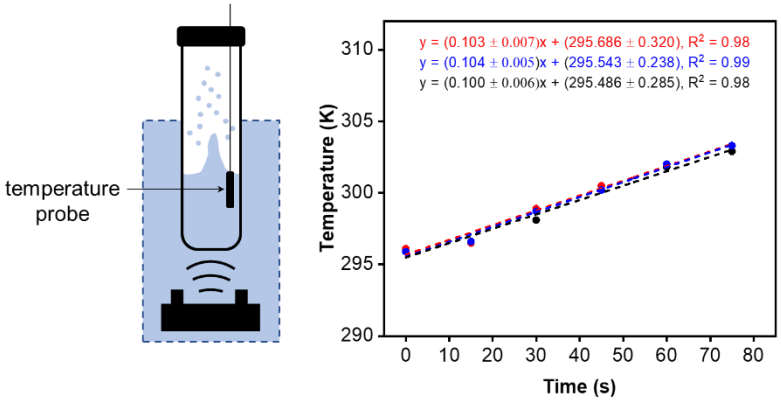

Figure A17. Experimental setup for determining the ultrasound absorbed by the water in the tube. Plot of temperature of 3 mL water versus exposure time with 1.7 MHz ultrasound.

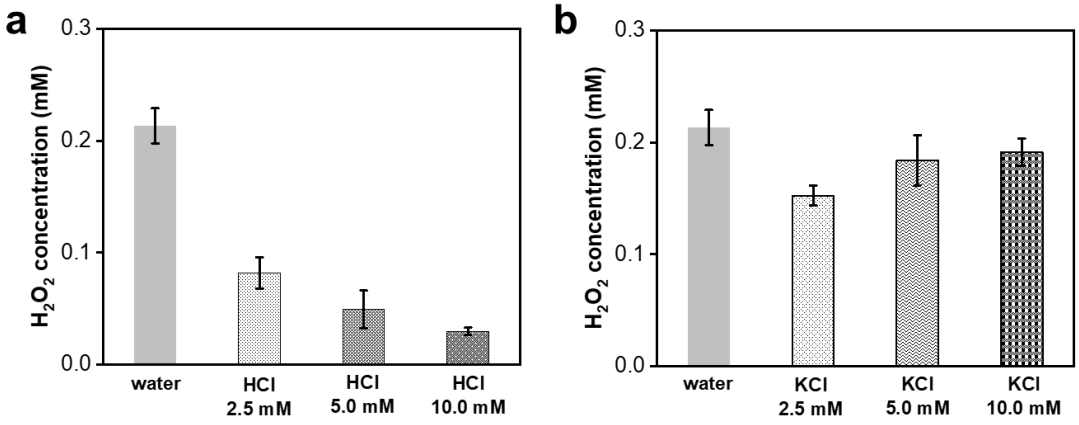

Figure A18. Effects of HCl and KCl concentrations on H_2O_2 formation under ultrasonic irradiation. After the cavities collapse, the radical products ($^{\bullet}OH$, $^{\bullet}H$, $^{\bullet}OOH$, etc.) diffuse into the bulk, react with nonvolatile solutes. For example, the Cl^- anion quenches $^{\bullet}OH$ radical faster under low pH or high Cl^- concentration conditions (see reference reactions in Table A4). Eventually, the $^{\bullet}OH$ radical concentration is lower, and less H_2O_2 product is produced. Reaction conditions: 3 mL of solutions were ultrasonically irradiated for 6 hours. After irradiation completed, H_2O_2 generated was characterized by PTO method.

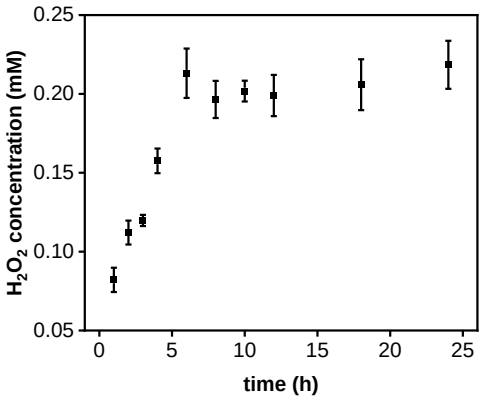

Figure A19. H_2O_2 production over ultrasonic irradiation time. Reaction conditions: 3 mL of water were irradiated with 1.7 MHz ultrasound. After irradiation completion, H_2O_2 generated was characterized by PTO method.

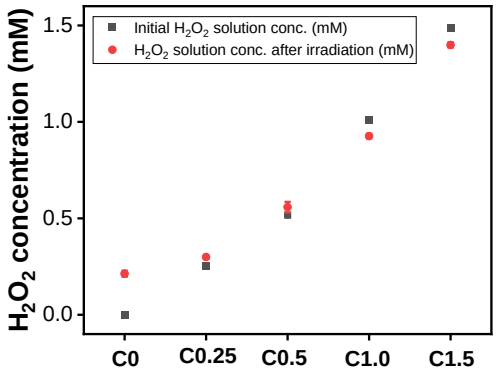

Figure A20. The average out of H_2O_2 concentration is due to the two competing processes. When the initial concentration of H_2O_2 is low, the recombination of $^{\bullet}OH$ radical is dominated, eventually more H_2O_2 is generated. When the initial concentration of H_2O_2 is

high, H_2O_2 effectively is consumed by the process of quenching •OH radical (see Equation 7 and 2 in Figure 10a). Reaction conditions: 3 mL of water with various initial H_2O_2 concentrations (C0 = 0 M, C0.25 = 0.25 M, C0.5 = 0.5 M, C1.0 = 1.0 M, and C1.5 = 1.5 M) were irradiated with 1.7 MHz ultrasound for 6 hours. After irradiation completion, H_2O_2 was characterized by PTO method.

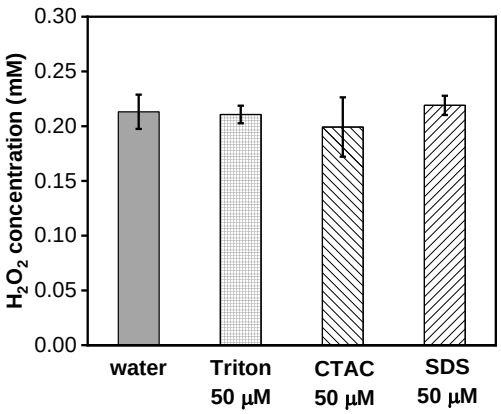

Figure A21. H_2O_2 production when irradiating Triton X-100, CTAC, and SDS solutions. Reaction conditions: irradiation of 3 mL of surfactant solutions with 1.7 MHz ultrasound for 6 hours. After irradiation completion, H_2O_2 was characterized by PTO method.

Tables

Table A4. Concentration of dissolved oxygen in water samples reported in Figure 3b. LaMotte™ dissolved oxygen kit (Winkler method) was used.

Water Sample	Dissolved oxygen (ppm)
N_2-purged	0.67 ± 0.07
air	7.90 ± 0.10
O_2-purged	~41[a]

[a]This value was calculated using Henry's law because the amount of dissolved oxygen exceeded the detection range of the test kit (0 – 10 ppm). According to Henry's law, the molar solubility of oxygen in water, $b_{O_2} = \frac{p_{O_2}}{K_{O_2}} = 12.8 \times 10^{-3} mol\ kg^{-1} = 41\ ppm$, where $p_{O_2} = 101.325\ (kPa)$ is the partial pressure of O_2 in the tube after 30-min

purging with oxygen, $K_{O_2} = 7.9 \times 10^4$ $(kPa\ kg\ mol^{-1})$ is the Henry's law constant for O_2 in water at 298 K.[7]

Table A5. Reaction rate constants of Cl^- reacting with •OH radical.[8, 9]

Reaction	$k_{forward}$	$k_{backward}$
$HO^{\cdot} + Cl^- \rightleftharpoons ClOH^{\cdot -}$	4.3×10^9 M^{-1} s^{-1}	6.1×10^9 s^{-1}
$ClOH^{\cdot -} + H^+ \rightleftharpoons Cl^{\cdot} + H_2O$	6.2×10^{12} s^{-1}	

References

1. Lee, J. K.; Han, H. S.; Chaikasetsin, S.; Marron, D. P.; Waymouth, R. M.; Prinz, F. B.; Zare, R. N., Condensing water vapor to droplets generates hydrogen peroxide. *P Natl Acad Sci USA* **2020,** *117* (49), 30934-30941.

2. Musskopf, N. H.; Gallo, A.; Zhang, P.; Petry, J.; Mishra, H., The Air-Water Interface of Water Microdroplets Formed by Ultrasonication or Condensation Does Not Produce H2O2. *J Phys Chem Lett* **2021,** *12* (46), 11422-11429.

3. Gallo, A.; Musskopf, N. H.; Liu, X. L.; Yang, Z. Q.; Petry, J.; Zhang, P.; Thoroddsen, S.; Im, H.; Mishra, H., On the formation of hydrogen peroxide in water microdroplets. *Chemical Science* **2022,** *13* (9), 2574-2583.

4. Sellers, R. M., Spectrophotometric Determination of Hydrogen-Peroxide Using Potassium Titanium(Iv) Oxalate. *Analyst* **1980,** *105* (1255), 950-954.

5. Thompson, L. H.; Doraiswamy, L. K., Sonochemistry: Science and engineering. *Ind Eng Chem Res* **1999,** *38* (4), 1215-1249.

6. Dulay, M. T., Huerta-Aguilar, C.A., Chamberlayne, C.F., Zare, R.N., Davidse, A. and Vukovic, S., Effect of relative humidity on hydrogen peroxide production in water droplets. *QRB Discovery QRB Discovery* **2021,** *2*.

7. Atkins, P. W., de Paula, J., *Physical chemistry*. 9th ed.; W.H. Freeman and Co.: New York, 2010.

8. Jayson, G. G., Parsons, B.J. and Swallow, A.J., Some simple, highly reactive, inorganic chlorine derivatives in aqueous solution. Their formation using pulses of radiation and their role in the mechanism of the Fricke dosimeter. *J. Chem. Soc., Faraday Trans., I, v. 69, no. 9, pp. 1597-1607* **1973**.

9. Kazmierczak, L., Wolszczak, M. and Swiatla-Wojcik, D., Ionic-Equilibrium-Based Mechanism of OH Conversion to Dichloride Radical Anion in Aqueous Acidic Solutions by Kinetic and Theoretical Studies. *J. Phys. Chem. B The Journal of Physical Chemistry B* **2019,** *123* (2), 528-533.

Appendix C

Standard Gibbs free energies of some reactions for H_2O_2 formation in water solution and gas phase. All data were extracted from Ref. 1[1].

$H_2O_{(l)} \rightarrow$ ½ $H_2O_{2(aq)}$ + ½ $H_{2(g)}$ (1)

$$\Delta G^\circ = \frac{1}{2}\left(\Delta G^\circ_{H_2O_2,aq} + \Delta G^\circ_{H_2,g}\right) - \Delta G^\circ_{H_2O,l}$$

$$= \frac{1}{2}(-134.1\ \text{kJ}\cdot\text{mol}^{-1} + 0\ \text{kJ}\cdot\text{mol}^{-1}) - (-237.1\ \text{kJ}\cdot\text{mol}^{-1})$$

$$= 170.0\ \text{kJ}\cdot\text{mol}^{-1} = 40.7\ \text{kcal}\cdot\text{mol}^{-1}$$

$H_2O_{(g)} \rightarrow$ ½ $H_2O_{2(g)}$ + ½ $H_{2(g)}$ (2)

$$\Delta G^\circ = \frac{1}{2}\left(\Delta G^\circ_{H_2O_2,g} + \Delta G^\circ_{H_2,g}\right) - \Delta G^\circ_{H_2O,g}$$

$$= \frac{1}{2}(-105.6\ \text{kJ}\cdot\text{mol}^{-1} + 0\ \text{kJ}\cdot\text{mol}^{-1}) - (-228.6\ \text{kJ}\cdot\text{mol}^{-1})$$

$$= 175.8\ \text{kJ}\cdot\text{mol}^{-1} = 42.1\ \text{kcal}\cdot\text{mol}^{-1}$$

$H_2O_{(l)}$ + ½ $O_{2(g)} \rightarrow H_2O_{2(aq)}$ (3)

$$\Delta G^\circ = \Delta G^\circ_{H_2O_2,aq} - \left(\Delta G^\circ_{H_2O,l} + \frac{1}{2}\Delta G^\circ_{O_2,g}\right)$$

$$= -134.1\ \text{kJ}\cdot\text{mol}^{-1} - \left(-237.1\ \text{kJ}\cdot\text{mol}^{-1} + \frac{1}{2}\times 0\ \text{kJ}\cdot\text{mol}^{-1}\right)$$

$$= 103.0\ \text{kJ}\cdot\text{mol}^{-1} = 24.6\ \text{kcal}\cdot\text{mol}^{-1}$$

$H_2O_{(l)} + O_{3(g)} \rightarrow H_2O_{2(aq)} + O_{2(g)}$ (4)

$$\Delta G^\circ = \left(\Delta G^\circ_{H_2O_2,aq} + \Delta G^\circ_{O_2,g}\right) - \left(\Delta G^\circ_{H_2O,l} + \frac{1}{2}\Delta G^\circ_{O_3,g}\right)$$

$$= (-134.1\ \text{kJ}\cdot\text{mol}^{-1} + 0\ \text{kJ}\cdot\text{mol}^{-1})$$

$$- \left((-237.1\ \text{kJ}\cdot\text{mol}^{-1}) + 163.2\ \text{kJ}\cdot\text{mol}^{-1}\right)$$

$$= -60.2\ \text{kJ}\cdot\text{mol}^{-1} = -14.4\ \text{kcal}\cdot\text{mol}^{-1}$$

References

1. James Speight, P. D., *Lange's Handbook of Chemistry, Sixteenth Edition*. 16th / ed.; McGraw-Hill Education: New York, 2005.